PRDX-1 Supports the Survival and Antitumor Activity of Primary and CAR-Modified NK Cells under Oxidative Stress

Marta Klopotowska[1,2,3], Malgorzata Bajor[2,3], Agnieszka Graczyk-Jarzynka[1,3], Agnieszka Kraft[4,5], Zofia Pilch[1], Andriy Zhylko[1,6], Malgorzata Firczuk[1], Iwona Baranowska[1,7], Michal Lazniewski[4,5], Dariusz Plewczynski[4,5], Agnieszka Goral[1], Karolina Soroczynska[1], Joanna Domagala[1], Katsiaryna Marhelava[1], Aleksander Slusarczyk[1], Kuba Retecki[1], Kavita Ramji[1], Marta Krawczyk[1], Madison N. Temples[8], Blanka Sharma[8], Mieszko Lachota[2,6], Herman Netskar[9], Karl-Johan Malmberg[9], Radoslaw Zagozdzon[2], and Magdalena Winiarska[1]

ABSTRACT

Oxidative stress, caused by the imbalance between reactive species generation and the dysfunctional capacity of antioxidant defenses, is one of the characteristic features of cancer. Here, we quantified hydrogen peroxide in the tumor microenvironment (TME) and demonstrated that hydrogen peroxide concentrations are elevated in tumor interstitial fluid isolated from murine breast cancers *in vivo*, when compared with blood or normal subcutaneous fluid. Therefore, we investigated the effects of increased hydrogen peroxide concentration on immune cell functions. NK cells were more susceptible to hydrogen peroxide than T cells or B cells, and by comparing T, B, and NK cells' sensitivities to redox stress and their antioxidant capacities, we identified peroxiredoxin-1 (PRDX1) as a lacking element of NK cells' antioxidative defense. We observed that priming with IL15 protected NK cells' functions in the presence of high hydrogen peroxide and simultaneously upregulated PRDX1 expression. However, the effect of IL15 on PRDX1 expression was transient and strictly dependent on the presence of the cytokine. Therefore, we genetically modified NK cells to stably overexpress PRDX1, which led to increased survival and NK cell activity in redox stress conditions. Finally, we generated PD-L1–CAR NK cells overexpressing PRDX1 that displayed potent antitumor activity against breast cancer cells under oxidative stress. These results demonstrate that hydrogen peroxide, at concentrations detected in the TME, suppresses NK cell function and that genetic modification strategies can improve CAR NK cells' resistance and potency against solid tumors.

Introduction

The interest in using natural killer (NK) cell–based strategies in human cancer immunotherapy has been growing, especially since the development of chimeric antigen receptors (CAR) and the promising development of CAR NK cells (1). The unique abilities of NK cells to precisely recognize and kill tumor cells without requiring prior immunization of the host and with tolerance to healthy cells makes them an attractive tool for treating cancer. Indeed, adoptive transfer of primary NK cells or irradiated NK cell lines, including the NK-92 cell line, has been reported to be feasible and safe in the treatment of patients with advanced malignancies (2). Several cytokine activation-based protocols are in development for *ex vivo* expansion of human primary NK cells to increase the number and activity of NK cells prior to and, most importantly, after infusion (3). Nevertheless, NK cell–based therapies are not free of certain limitations. Despite clinical responses in some patients, the immunosuppressive tumor microenvironment (TME), an acidified, hypoxic compartment deprived of nutrients, filled with metabolite byproducts, and characterized by chronic oxidative stress, is challenging to overcome for the antitumor activity of NK cells (4).

Oxidative stress is caused by the imbalance between an increased generation of reactive oxygen species (ROS) and their removal by antioxidant defenses. Physiologically, ROS are natural byproducts of aerobic metabolism and are involved in various processes, including the electron transport chain in the mitochondria, gene expression, signal transduction, and activation of transcription factors. Among biologically relevant ROS ($^1O_2$, $O_2^{\bullet-}$, H_2O_2 $OH^{\bullet}$, $ONOO^-$, HOCl, HOBr), hydrogen peroxide (H_2O_2) has the highest stability and highest intracellular concentration (5). It undergoes facilitated and regulated diffusion across organelle and plasma membranes through aquaporin (AQP) channel transporters (6). Once transported into the cell, H_2O_2 can be neutralized by intracellular antioxidant defenses, such as low-molecular-weight thiols—mainly glutathione (GSH)—and various

[1]Department of Immunology, Medical University of Warsaw, Warsaw, Poland. [2]Department of Clinical Immunology, Medical University of Warsaw, Warsaw, Poland. [3]Laboratory of Immunology, Mossakowski Medical Research Institute, Polish Academy of Sciences, Warsaw, Poland. [4]Laboratory of Functional and Structural Genomics, Centre of New Technologies, University of Warsaw, Warsaw, Poland. [5]Faculty of Mathematics and Information Science, Warsaw University of Technology, Warsaw, Poland. [6]Doctoral School, Medical University of Warsaw, Warsaw, Poland. [7]Department of Renal and Body Fluid Physiology, Mossakowski Medical Research Institute, Polish Academy of Sciences, Warsaw, Poland. [8]J. Crayton Pruitt Family Department of Biomedical Engineering, University of Florida, Gainesville, Florida. [9]Department of Cancer Immunology, Institute for Cancer Research, The Norwegian Radium Hospital, Oslo University Hospital, Oslo, Norway.

Note: Supplementary data for this article are available at Cancer Immunology Research Online (http://cancerimmunolres.aacrjournals.org/).

Corresponding Author: Magdalena Winiarska, Department of Immunology, Medical University of Warsaw, Nielubowicza 5 Street, 02-097 Warsaw, Poland. Phone: 4822-599-21-72; Fax: 4822-599-21-94; E-mail: mwiniarska@wum.edu.pl

Cancer Immunol Res 2022;10:228–44

doi: 10.1158/2326-6066.CIR-20-1023

antioxidant enzymes. Catalase (CAT) and glutathione peroxidases (GPX), which catalyze the reduction of H_2O_2 at the expense of GSH, and peroxiredoxins (PRDX), which are restored to the reduced state by thioredoxins (TXN) and thioredoxin reductases (TXNRD; ref. 7) comprise a major part of the antioxidant defense.

Within the TME, ROS are produced by cancer cells, as well as by immune cells, such as tumor-associated macrophages (TAM), myeloid-derived suppressor cells (MDSC), and neutrophils (8). Increased ROS production by cancer cells, compared with normal tissue, is mainly the result of metabolic alterations, such as increased oxidative phosphorylation in mitochondria (9). Increased ROS, characteristic especially of triple-negative breast cancer cells, are necessary for tumor cell survival (10). In turn, in TAMs, MDSCs, and neutrophils, $O_2^{\bullet-}$ and H_2O_2 are predominantly produced by NADPH oxidase 2 (NOX2; ref. 11) and can be further utilized by peroxidases to generate hypochlorous acid and other oxidants. It has also been shown that H_2O_2 triggers DNA damage and increased mutagenesis during tumorigenesis (12). Besides promoting oncogenesis, excessive ROS exhibit immunosuppressive activity (13, 14) by inducing NK cell death and impairing NK cell–mediated tumor immunosurveillance (15–18). Several reports demonstrated in tumors an accumulation of $CD56^{bright}$ NK cells, responsible for cytokine production and immune response regulation, at the expense of potent cytotoxic $CD56^{dim}$ NK cells (18, 19). However, the mechanisms explaining the uniquely high sensitivity of NK cells to oxidative stress are not entirely clear.

Therefore, in our study, we aimed to identify and augment deficiencies in NK cells' antioxidative defense system in order to promote their activity in the postinfusion conditions of oxidative stress within the TME. We first performed a comparison of T, B, and NK cells' sensitivities to redox stress and thereafter examined various mechanisms involved in their antioxidant capacities. We identified PRDX1 as a downstream effector of importance for protecting NK cells against oxidative stress. Based on these findings, we generated PD-L1–CAR NK cells and modified them with PRDX1 to enhance their antitumor activity against breast cancer cells. We believe this genetic modification-based strategy may pave the way for more effective NK cell–based therapeutics against solid tumors.

Materials and Methods

Cell culture

Human NK cell lines NK-92 (a generous gift from Prof. Kerry Campbell, Fox Chase Cancer Center, Philadelphia) and NK-92MI (a generous gift from Prof. Daniel Olive, Centre de Recherche en Cancérologie de Marseille, Inserm, U1068, CNRS, UMR7258, Institut Paoli-Calmettes, Aix-Marseille University, UM 105, Marseille, France) were cultured in X-VIVO 20 medium (Lonza) supplemented with 5% human serum (Sigma-Aldrich) and penicillin (100 U/mL) and streptomycin (100 μg/mL; Sigma-Aldrich). For some experiments, the cells were maintained in RPMI-1640 medium (GIBCO) supplemented with 10% heat-inactivated bovine calf serum (HyClone), 2 mmol/L L-glutamine (Sigma-Aldrich), and a mixture of penicillin (100 U/mL) and streptomycin (100 μg/mL; Sigma-Aldrich; further described in the text as the full RPMI-1640). Human breast carcinoma cell lines MCF-7 (86012803) and MDA-MB-231 (92020424) were purchased from the European Collection of Authenticated Cell Culture; SK-BR-3 (HTB-30) was purchased from the American Type Culture Collection (ATCC). The cells were maintained the RPMI-1640 full medium. Chronic myelogenous leukemia cell line K562 (CCL-243) was obtained from ATCC and cultured in the full RPMI-1640 medium. HEK293T (CRL-3216) cells were purchased from ATCC and were cultured in DMEM supplemented with 10% bovine calf serum (HyClone). The murine breast mammary carcinoma 4T1 (CRL-2539), EMT6 (CRL-2755), and EO771 (CRL-3461) cell lines purchased from ATCC were maintained in the full RPMI-1640. Cells were cultured at 37°C, 5% CO_2, in a humidified atmosphere. Human cell lines were authenticated using PCR-single-locus-technology (Eurofins Genomics). Cells were maintained in culture for approximately two months during experimental use and were regularly tested for *Mycoplasma* contamination using the PCR method.

Mice

Female wild-type Balb/c and C57BL/6 mice were purchased from the Animal House of the Polish Academy of Sciences, Mossakowski Medical Research Institute (Warsaw, Poland). NOD.Cg-Prkdc<scid>Il2rg<tm1Wjl>/SzJ (NSG) mice were obtained from the Charles River Laboratories and were bred at the animal facility of the Department of Immunology, Medical University of Warsaw. Randomization of groups was not required in these animal model studies. Experiments were performed at the Animal Facility of the Medical University of Warsaw. Tumor size volume 1,500 mm^2 was predetermined as a humane endpoint. During the study, none of the mice experienced unintended discomfort requiring intervention to alleviate the suffering. All *in vivo* experiments and specific procedures and protocols used for this study were performed in accordance with the guidelines and approved by The Second Local Ethics Committee for the Animal Experimentation, Warsaw University of Life Sciences (number: WAW2/111/2019, WAW2/005/2021, and WAW2/074/2021). The investigator was not blinded when assessing the outcome, as blinding was not relevant to this study.

Tumor model for tumor interstitial fluid collection

Tumors were generated in Balb/c (4T1 and EMT6 murine cell lines: 3.5×10^5 cells), C57BL/6 (EO0771 murine cell line: 3.5×10^5 cells), and NSG (MDA-MB-231: 2×10^6 cells; MCF-7: 3×10^6 human cell lines; and 4T1: 3.5×10^5 murine cell line) mice by subcutaneous inoculation of tumor cells in 100 μL of a mixture of PBS:Matrigel Growth Factor Reduced (Corning, LifeSciences; 1:1), on the right flank. MCF-7 cell administration was preceded by subcutaneous implantation of estrogen pellets (17β-ESTRADIOL pellets, 0.36 mg/pellet, Innovative Research of America), 4 days before tumor cell inoculation. MCF-7 cells were injected into the mammary fat pad in 50 μL of a mix of PBS: Matrigel (1:1). Tumors were measured with a caliper, and tumor size was calculated as their surface, according to the formula: $(mm^2) = (\text{length [mm]}) \times (\text{width [mm]})/2$. When one dimension of the tumor reached 15 mm, the tumor was used for tumor insterstitial fluid (TIF) and subcutaneous fluid (SCF) isolation.

Collection of TIF by ultrafiltration

Mice were anesthetized by administrating 10 mg ketamine and 1.5 mg xylazine per 100 g body weight. The UF-1-2 *In Vivo* Ultrafiltration Sampling Probes (BASI, MF-7027) probe was implanted centrally into the tumor masses for two hours to collect tumor secretomes. To extract fluid from the extracellular space of healthy tissue ultrafiltration (UF) probe was implanted under the skin at the opposite side to the tumor location. High-molecular-weight compounds, such as proteins, were excluded from the analytes by a filtration membrane. After ultrafiltration, approximately 10 μL of TIF and 12 to 18 μL of SCF was obtained, and an appropriate volume was used for H_2O_2 measurement by Hydrogen Peroxide Assay Kit (Abcam; ab102500) according to the manufacturer's specifications.

Blood sampling from mice

Before UF probe implantation, blood was collected by using the submandibular vein method. After a quick puncture of the vein, the blood drops exuded from the puncture point were collected into a tube with EDTA (The Vet-Tube Range). Samples were spin down for 15 minutes at 700 × *g*, at 25°C, and 100 μL of freshly isolated plasma was placed into a column with a 30 kDa cutoff (Amicon Ultra 0.5 mL Centrifugal Filters, Millipore). After ultrafiltration, approximately 50 μL of the plasma passed through the columns, and an appropriate volume of pure plasma was taken for H_2O_2 measurement by the Hydrogen Peroxide Assay Kit (Abcam; ab102500).

Tumor immunophenotyping

Tumors were cut into small pieces and digested for 30 minutes at 37°C using Collagenase type IV (600 U; Sigma-Aldrich), and DNase (400 U; Sigma-Aldrich). Next, tissue fragments were dissociated using a gentleMACS Dissociator and filtered through a 100-μm cell strainer, then washed with PBS containing 2 mmol/L EDTA and 1% FCS, centrifuged, and stained. For staining, cells were blocked in 5% normal rat serum and stained with fluorescently labeled monoclonal antibodies.

Flow cytometry antibodies

Flow-cytometric analyzes were performed using BD LSRFortessa X20 instrument (BD Biosciences), BD FACSCantoII flow cytometer or BD LSR II (BD Biosciences). Data were analyzed with FlowJo (Tree Star). Antibodies to the following mouse proteins were used for flow cytometry: CD45.2 (BD Horizon, clone 104,), CD11b (eBioscience, clone M1/70), Ly6C (eBioscience, clone HK1.4), Ly6G (BioLegend, clone 1A8), CD11c (eBioscience, clone N418), MHC-II (eBioscicence, clone M5/114.15.2), F4/80 (BioLegend, clone BM8), CD4 (eBioscience, clone GK1.5), and CD8a (eBioscience, clone 53-6.7). To assess the live versus dead status of isolated cells, they were stained with Zombie NIR Fixable Viability Kit (BioLegend) according to the manufacturer's protocol.

FACS sorting

NK cells were sorted into two major subsets, based on CD56 expression into $CD56^{bright}$ and $CD56^{dim}$. Briefly, NK cells isolated from peripheral blood mononuclear cells (PBMC) were rested overnight. The next day, NK cells were stained with the following antibodies CD56 (clone AF12-7H3, Miltenyi Biotec) or CD56 (clone R19-760, BD Pharmingen). Cell sorting was performed with FACSAria III cell sorter (BD Biosciences).

Reagents

Glucose oxidase (GOX), sodium L-ascorbate (L-ASC), L-dehydroascorbate (L-DHA), and CAT were obtained from Sigma-Aldrich. The reagents were dissolved in sterile distilled water and diluted in a culture medium before an experiment. Torin-1 was purchased from Selleckchem, dissolved in DMSO, and diluted in a culture medium. H_2O_2 was either ordered from Sigma-Aldrich or H_2O_2 included in Hydrogen Peroxide Assay Kit (Abcam; ab102500). Trastuzumab (Kanjinti) leftover was donated by patients.

Primary cell isolation

Human primary T cells, B cells, and NK cells were isolated from buffy coats from healthy volunteers obtained from the Regional Blood Center in Warsaw, Poland, with the knowledge of the Bioethics Committee of Medical University of Warsaw, Poland. PBMCs were isolated by density gradient separation using Lymphoprep (STEMCELL Technologies Canada, Inc.). T cells, B cells, and NK cells were isolated using the EasySep Human T-cell Enrichment Kit, EasySep Human B-cell Enrichment Kit, or EasySep Human NK cell Enrichment Kit (STEMCELL Technologies Canada, Inc.) according to the manufacturer's protocols. Primary cells were cultured in full RPMI-1640 medium unless otherwise described for specific experimental procedures.

Primary cell activation

For NK cell stimulation, the cells were seeded at cell density 1×10^6 cells/mL with 10 ng/mL of human recombinant IL15 (Miltenyi Biotec) or with 500 U/mL of human recombinant IL2 (Proleukin; Novartis) and CD2/NKp46 MACSiBead Particles from NK Cell Activation/Expansion Kit (Miltenyi Biotec; 130-094-483). For T-cell activation, the Dynabeads Human T-Activator CD3/CD28 (Thermo Fisher Scientific) simultaneously with 30 U/mL of IL2 were used. B cells were activated by coculture with mitomycin-treated HT1080 cells overexpressing CD40 ligand (CD40L; ref. 20) and 100 ng/mL of IL21 (PeproTech).

Torin-1 treatment

Human primary T cells, B cells, and NK cells were seeded at the density of 0.5×10^6 cells/mL onto 96-well plates. Torin-1 (final concentration 1 μmol/L) or an equal volume of DMSO (0.1%) was added to the wells. Subsequently, the cells were stimulated with IL15 (10 ng/mL) for 1 and 3 days. NK-92 cells were starved of IL2 for 24 hours before use in an experiment. The cells were seeded onto a 24-well plate at a cell density of 0.25×10^6 cells/mL. Then, Torin-1 or DMSO was added to the wells, and appropriate groups were stimulated with 10 ng/mL of IL15 for 48 hours.

Assessment of cell survival upon prooxidant treatment

Human primary T cells, B cells, and NK cells were seeded at 0.5×10^6 cells/mL onto 96-well plates (primary cells). H_2O_2, GOX, L-ASC, L-DHA were added for 16 hours. Subsequently, the viability of the primary cells was assessed by propidium iodide (PI, 1 μg/mL, Sigma-Aldrich) staining, BD Horizon Fixable Viability Stain–FVS510 (BD Biosciences), LIVE/DEAD Fixable Aqua Dead Cell Stain Kit (Thermo Fisher Scientific) or Zombie NIR Fixable Viability Kit (BioLegend). Cells were analyzed using either BD FACSCantoII flow cytometer or BD LSR II (BD Biosciences). To assess the specificity of the cytotoxic effect of H_2O_2, GOX, and L-ASC on cell viability, the cells were pretreated for 30 minutes with catalase (100 μg/mL) before the addition of the compounds. Viability of mRNA-electroporated human primary NK cells in GOX conditions (16 hours) was assessed with either PI or LIVE/DEAD Fixable Aqua Dead Cell Stain, whereas viability of NK-92MI-mRFP, NK-92MI-PRDX1-mRFP, CAR-PDL-1-NK-92MI-mRFP, and CAR-PD-L1-PRDX1-NK-92MI cell lines after incubation with GOX for 20 hours (0.125×10^6 cells/mL in 48-well plates) was evaluated by FVS510 or ZOMBI NIR staining, and all were analyzed with flow cytometry.

Cell-surface free thiol staining

Free surface thiol groups were determined using the Alexa Fluor 647 C2 Maleimide dye (Thermo Fisher Scientific). Freshly isolated PBMCs were incubated with 5 μmol/L Alexa Fluor 647 C2 Maleimide dye for 15 minutes on ice. The cells were washed and resuspended in staining buffer (PBS supplemented with 2% FBS and 1 mmol/L EDTA) and stained for 20 minutes on ice with the following antibodies: CD56 (clone R19-760, BD Pharmingen), CD3 (SK7, BD Pharmingen), CD19 (SJ25C1, BD Pharmingen), and FVS510. After washing, cells were analyzed on BD FACSCanto II flow cytometer.

Intracellular free thiol staining

Intracellular thiols were assessed with ThiolTracker Violet reagent (Invitrogen). Primary T cells, B cells, and NK cells were seeded onto a U-bottom 96-well plate at a cell density of 0.5×10^6 cells/mL and were rested overnight. The next day cells were stained with 2 μmol/L of ThiolTracker Violet reagent at 37°C and 5% CO_2 for 30 minutes. Subsequently, the cells were washed in PBS and analyzed on BD LSRFortessa X20 instrument (BD Biosciences) and HTS sampler. The experiment was performed in two technical replicates for every donor.

Assessment of H_2O_2 concentration in medium

Different concentrations of GOX were added to the full RPMI-1640 in a U-bottom 96-well plate and were incubated for 4 hours. H_2O_2 concentration in the medium was measured using the Hydrogen Peroxide Assay Kit (Abcam) according to the manufacturer's protocol. Briefly, 50 μL of H_2O_2 standards were plated in a black 96-well flat bottom plate with a transparent bottom. The GOX-treated medium (20–30 μL) was aspirated and diluted in assay buffer and added to the wells. Thereafter, OxiRed/HRP mix diluted in assay buffer was added to the wells and incubated for 10 minutes at room temperature. Both fluorimetric (EnVision, PerkinElmer) and colorimetric readout (ASYS UVM340 Microplate Reader) were taken.

Detection of intracellular ROS

Primary T, B, and NK cell subpopulations were incubated with 1 μmol/L CM-H_2-DCFDA fluorescent probe (Molecular Probes) in PBS at 37°C and 5% CO_2 for 30 minutes and then washed with the culture medium. Next, the cells were seeded onto U-bottom 96-well plates at a cell density of 5×10^5 cells/mL and incubated with 5 or 10 μmol/L H_2O_2 for 1 hour. To determine the intracellular ROS concentration, the cells were analyzed using BD FACSCantoII flow cytometer (BD Biosciences). Results were shown as geometric mean fluorescence intensity of oxidized CM-H_2-DCFDA. For the CellROX Deep Red and CellROX Green assays (Thermo Fisher Scientific), resting T, B, and NK cells were seeded onto U-bottom 96-well plates at the density of 5×10^5 cells/mL and incubated with 5 or 10 μmol/L H_2O_2 for 1 hour. Subsequently, the CellROX Deep Red/CellROX Green reagent was added to the cells and the staining was performed at 37°C, 5% CO_2 for 30 minutes. After washing, the cells were analyzed on BD LSRFortessa X20 instrument (BD Biosciences).

Real-time cell analysis cytotoxicity assay

The cytotoxicity of NK cells was assessed with a real-time cell analysis (RTCA) assay. Adherent target MCF-7 (3×10^4 cells/well), MDA-MB-231 (3×10^4 cells/well), or SK-BR-3 (4×10^4 cells/well) cells were seeded onto 16-well E-Plates (ACEA Biosciences) in 150 μL of standard RPMI-1640 full medium. For nonadherent K562 cells, 16-well E-Plates were precoated with the Liquid Tumor Killing Assay (anti-CD71) Tethering Kit (ACEA Biosciences) according to the manufacturer's recommendations. K562 cells were seeded onto 16-well E-Plates at a cell density of 1.5×10^4 cells/well. The proliferation of target cells was monitored in the incubator at 37°C (5% CO_2, 95% humidity) for 24 hours with the xCELLigence impedance-based RTCA system (Acea Biosciences). The next day, 100 μL of the medium was aspirated and replaced with the medium containing effector cells (human primary NK cells or NK-92 cell lines) at different effector to target (E:T) ratios. For antibody-dependent cell cytotoxicity (ADCC) assays, trastuzumab (anti-HER2 antibody) was added to appropriate wells at a final concentration of 10 μg/mL. The cells were monitored for the next 20 to 24 hours. Analysis was performed using RTCA Software Pro (ACEA Biosciences). The impedance changes (cell index) were normalized to the end value of the target cells' proliferation and plotted over time as normalized cell index.

RNA isolation and quantitative real-time PCR

Total RNA from primary cells was isolated with the use of either the High Pure RNA Isolation Kit (Roche Diagnostics) or RNase Mini Kit (Qiagen) with QIAshredder (Qiagen) used for homogenization of cells lysates according to the manufacturer's recommendation. The concentration of isolated RNA was measured with the spectrophotometer NanoDrop 2000 (Thermo Scientific). In each experiment, equal amounts of RNA (from 200 ng to 500 ng) were used for reverse transcription (RT) to complementary cDNA using SuperScript IV Reverse Transcriptase (Thermo Fisher Scientific). RT reaction was performed according to the manufacturer's recommendations. Briefly, random hexamers annealing was performed at 65°C for 5 minutes and cooled on ice. Then RT reaction mix was preincubated with annealed RNA at room temperature for 10 minutes and incubated at 55°C for 10 minutes, followed by enzyme inactivation at 80°C for 10 minutes. Quantitative real-time PCR (qPCR) was performed using LightCycler 480 SYBR Green I Master (Roche Diagnostics) and LightCycler 480 II device (Roche Diagnostics). The qPCR temperature cycling conditions were as follows: initial denaturation at 95°C for 5 minutes, 45 standard amplification cycles of denaturation at 95°C for 10 seconds, primer annealing at 60°C for 10 seconds, and primer extension at 72°C for 10 seconds, followed by melting curve analysis (95°C for 5 seconds, 65°C for 1 minute 97°C continuous) and cooling at 40°C for 30 seconds. Samples were measured in duplicates in each PCR run. RPL29 (ribosomal protein L29) and β-2-microglobulin were used as reference genes. Sequences of all primers used in qPCR are presented in **Table 1**. For the assessment of aquaporin 3 (AQP3) and aquaporin 11 (AQP11) in primary human NK, T, and B cells, the TagMan assays were used. The qRT-PCR was performed with TaqMan Fast Advanced Master Mix (Thermo Fisher Scientific) and the following TaqMan Gene-Expression Assays: AQP3 (Hs00185020_m1) and AQP11 (Hs00542682_m1) according to the manufacturer's recommendations. For the reference gene, GAPDH (Hs02786624_g1) was used.

Western blotting

For Western blotting (WB), cells were lysed with lysis buffer (50 mmol/L Hepes, 150 mmol/L NaCl, 5 mmol/L EDTA, 1% Triton X-100, 10% glycerol, pH 7.4) or Cell Lysis Buffer (Cell Signaling Technology) supplemented with Complete Protease Inhibitor Cocktail and Phosphatase Inhibitor Cocktail (Roche Diagnostics). Protein concentration was measured using the Pierce BCA Protein Assay Kit (Thermo Fisher Scientific) according to the manufacturer's instructions with minor modifications on the ASYS UVM340 Microplate Reader (Biochrom). Cell lysates (15–30 μg) were separated in 12% polyacrylamide gel, then transferred onto Protean nitrocellulose membranes and blocked with either 5% nonfat milk or 5% Bovine Serum Abumine (Kenilworth) in TBST (Tris-buffered saline, pH 7.4 and 0.05% Tween 20) and then incubated with the following primary antibodies PRDX1 (catalog number HPA007730, Sigma-Aldrich; dilution 1:1,000), TXN1 (2429, Cell Signaling Technology; dilution 1:1,000), GPX1 (3206, Cell Signaling Technology dilution 1:1,000), CAT (12980, Cell Signaling Technology; dilution 1:1,000), SOD1 (2770, Cell Signaling Technology; dilution 1:1,000), and β-actin (A222, Sigma-Aldrich; dilution 1:50,000). For detection of primary protein bands, HRP-conjugated secondary antibodies and the Super Signal chemiluminescent substrates (Thermo Fisher Scientific) were used. The signal was detected using the ChemiDoc Imaging System (Bio-Rad Laboratories). Densitometry of WBs was calculated using the Image Lab Software (Bio-Rad Laboratories).

Table 1. List and sequences of all primers used in qPCR.

Primer	Forward sequence (5′→ 3′)	Reverse sequence (5′→ 3′)
PRDX1	CACTGACAAACATGGGGAAG	TTTGCTCTTTTGGACATCAGG
TXN1	TAAAGGGAGAGAGCAAGCAG	CAGAGAGGGAATGAAAGAAAGG
TXNRD1	TCACCCCAGTTGCAATCC	GGTTGGAACATTTTCATAGTCACA
CAT	AGAGAAATCCTCAGACACATC	CAGCTTGAAAGTATGTGATCC
SOD1	AATGGACCAGTGAAGGTGTGGGG	CACATTGCCCAAGTCTCCAACATGC
GPX1	ACGATGTTGCCTGGAACTTTGAG	CTCGATGTCAATGGTCTGGAAG
GSR	ATGGTCTGTGCTAACAAGGAA	GTTGCTCCCATCTTCACTGCA
RPL29	CAGCTCAGGCTCCCAAAC	GCACCAGTCCTTCTGTCCTC
β-2microglobulin	TGGAGGCTATCCAGCGTACT	CGGATGGATGAAACCCAGAC

CAR constructs

The anti-CD19 CAR construct was a generous gift from Dr. Jon-Amund Kyte from Oslo University Hospital under the MTA agreement. The construct comprises an anti-CD19 single-chain fragment variable fragment (scFv) derived from the FMC63 mouse hybridoma, an IgG1-CH2CH3 spacer region, and the two costimulatory domains CD28 and OX40 and was subcloned into the mRNA expression vector pCIpA102. The anti–PD-L1 CAR was synthesized by Creative Biolabs. The scFv is based on the atezolizumab sequence and was combined with a second-generation CAR backbone comprised of IgG4 hinge region, CD28 transmembrane and signaling portions, and CD3ζ signaling domain. PD-L1 CAR was cloned into the BamHI/SbfI restriction sites of the lentiviral transfer plasmid pSEW (21), thereby replacing the *gfp* gene. CAR expression in the cells, after transduction or electroporation was assessed with AF647 goat anti-human IgG, F(ab')2 fragment specific antibody (cat. no. 109-605-006, Jackson Immuno-Research Europe Ltd.) or AF647 goat anti-human IgG Fcγ fragment–specific antibody, for PD-L1 CAR (cat. no. 109-606-098 Jackson Immuno-Research Europe Ltd.).

mRNA synthesis

mRNA for PRDX1 and CAR-CD19 was synthesized *in vitro* with the use of the RiboMAX Large-Scale RNA Production System (Promega). The *PRDX1* coding sequence was subcloned from PRDX1-pETMM11 plasmid to mRNA expression vector pCIpA102 (kindly provided by Dr. Stein Sæbøe-Larssen from Oslo University Hospital) with the use of FastDigest EcoRI and NotI restriction enzymes (Thermo Fisher Scientific). pCIpA102 plasmid containing CAR-CD19 coding sequence was kindly provided by Dr. Jon Amund Kyte Oslo University Hospital under MTA. Both plasmids pCIpA102-PRDX1 and pCIpA102-CAR-CD19 were linearized with MfeI restriction enzyme (New England BioLabs) and used for the mRNA synthesis reaction. Anti-Reverse Cap Analog (Trilink Biotechnologies) was used to cap the mRNA. The synthesis reaction was carried out for 4 hours at 37°C. Then, RNA-free DNase was added to digest the residual DNA matrix. The synthesized mRNA was then purified using either the MEGAclear Transcription Clean-Up Kit (Thermo Fisher Scientific) or the lithium chloride (LiCl; Thermo Fisher Scientific) precipitation method. The mRNA's quality and quantity were assessed by agarose gel electrophoresis and NanoDrop (Thermo Scientific).

mRNA electroporation

For mRNA electroporation, primary NK cells were cultured in SCGM medium (CellGenix) supplemented with 5% human serum and the mixture of antibiotics for 3 days in the presence of IL15 (10 ng/mL). After that, NK cells were washed and resuspended in serum and antibiotics-free SCGM medium at a cell density of 10–15 × 10^6 cells/mL. mRNA was mixed with the cell suspension at the final mRNA concentration of 100 mg/mL. Subsequently, the cell suspension was placed in a 4-mm gap cuvette and electroporated with 500 V for 2 ms using a BTX 830 Square Wave Electroporator (BTX Technologies) or Gene Pulser Xcell (Bio-Rad) and square wave settings. After electroporation, cells were immediately transferred to a prewarmed culture medium supplemented with 5% human serum and IL15 (10 ng/mL) and then cultured overnight. NK-92MI cells were electroporated using Gene Pulser Xcell electroporator (Bio-Rad). The cells were placed in a 4-mm gap cuvette in 250 μL of empty RPMI-1640 and electroporated with 300 V, 150 μF, 200 Ω. After electroporation, cells were transferred to prewarmed RPMI supplemented with 10% FCS.

Generation of NK-92 cells stably overexpressing PRDX1

PRDX1 overexpression was done in NK-92MI using a lentiviral transduction system. The original plasmid HIV-SFFV-mRFP-WPRE CORRIGE (a kind gift from Prof. Els Verhoeyen, University of Lyon) was modified by replacing the mRFP with the MCS-IRES-mRFP sequence. The *PRDX1* sequence was amplified by PCR from PRDX1-pETMM11 plasmid and cloned into MCS (multicloning site) by ligation into BamHI and MluI sites (FastDigest Thermo Fisher Scientific). The sequence of the construct (HIV-SFFV-PRDX1-IRES-mRFP) was confirmed by DNA sequencing. NK-92MI cells were modified with lentiviral transduction, as described below. After transduction, cells were sorted based on mRFP fluorescence. The sorting was performed with FACSAria III cell sorter (BD Biosciences). The overexpression of PRDX1 was confirmed by WB. NK-92MI cells modified with empty plasmid HIV-SFFV-IRES-mRFP are referred to NK-92MI-mRFP cells, whereas NK-92MI cells with PRDX1 overexpression (HIV-SFFV-PRDX1-IRES-mRFP) are referred to NK-92MI-PRDX1-mRFP.

Generation of NK-92 cells stably expressing luciferase

The NK-92 cell line was modified using the plasmid (pSLIEW-luc-GFP kindly provided by Prof. Olaf Heidenreich; ref. 22) allowing cells to express both firefly luciferase and eGFP. eGFP-positive cells were sorted with FACSAria III cell sorter (BD Biosciences).

In vivo imaging of NK-92MI cells overexpressing luciferase in the tumor

Ten days after tumor cell inoculation, mice received 5.0 × 10^6 of either NK-92MI-mRFP-pSLIEW-luc cells or NK-92MI-PRDX1-mRFP-pSLIEW-luc cells intratumorally. Immediately following the injection of NK-92MI cells, bioluminescence imaging (BLI) was performed with 100 μL of d-luciferin (Syd Labs; 150 mg luciferin/kg body weight). The NK cell imaging was performed using the IVIS Imaging System (Xenogen). Images were analyzed with the Living Image 4.3 software package (Caliper Life Science). To quantify the BLI signal of NK-92MI cells, the

regions of interest were drawn on the tumor region, and the results were used to generate the BLI data presented as total flux (photons/second).

Luciferase-based *in vitro* proliferation of NK-92MI cells

NK-92MI-mRFP and NK-92MI-PRDX1-mRFP cells previously modified to overexpress firefly luciferase were seeded at a cell density of 5×10^4/mL onto a 12-well plate in the full RPMI medium. Every day the cells were resuspended and 100 μL of the cell suspension was aspirated and transferred onto a new black 96-well black plates with a clear bottom (PerkinElmer). Subsequently, 100 μL of Bright-Glo Luciferase Assay System (cat. No. E2610, Promega) was added to the wells and the plate was incubated for 5 minutes in darkness, then the bioluminescence signal was measured using Victor Plate Reader (PerkinElmer). Cell proliferation was monitored for 7 days.

PD-L1 knockout in MDA-MB-231 cells

Lentiviral plasmid lentiCRISPR v2 containing the sequences encoding Cas9 nuclease and the single guide RNA (sgRNA) scaffold was a gift from Feng Zhang (Addgene, #52961). The sgRNA sequence targeting human PD-L1 (ACATGTCAGTTCATGTTCAG) was selected from the Human CRISPR Knockout Pooled Library Brunello database and subcloned into the lentiCRISPR v2 vector using a pair of oligonucleotides:

Forward 5′-CACCGACATGTCAGTTCATGTTCAG-3′
Reverse 5′-AAACCTGAACATGAACTGACATGTC-3′

As a control, lentiCRISPR v2 plasmid with a nontargeting sgRNA sequence sgNTC (ACGGAGGCTAAGCGTCGCAA) was used. After the viral transduction, the modified MDA-MB-231 cells were selected based on their antibiotic resistance to puromycin delivered by lentiCRISPR v2 vector. Surface PD-L1 expression was evaluated by flow cytometry using anti–PD-L1 clone MIH1 (Thermo Fisher Scientific #17-5983-42, dilution 1:100).

NK-92 infiltration into tumors

To evaluate NK cell infiltration into tumors, a previously established three-dimensional (3D) lung tumor model (23) was used that recapitulates the immunosuppressive characteristics of lung tumors *in vivo*. The 3D models were engineered from poly(ethylene glycol) (PEG)-based hydrogels functionalized with both cell-adhesive and enzymatically degradable peptides as described previously (23). Briefly, 10 million cells/mL DiO-labeled A549 human lung cancer cells (ATCC) were photoencapsulated in 10 μL of the PEG-based precursor solution dissolved in PBS with 0.05% (v/v) Irgacure 2959 (photoinitiator). The hydrogel precursor solution contained a 50:50 ratio of 10% (w/v) PEG-diacrylate (Laysan Bio Inc) and 10% (w/v) PEG functionalized with matrix metalloproteinase (MMP) degradable sites (sequence GGVPMS↓MRGGK, Biomatik), and 5 mmol/L of PEG functionalized with cell adhesion sites (arginine-glycine-aspartic acid, RGD, Vivitide). The 3D models were polymerized by OmniCure S2000 light (Excelitas Technologies, Corp.) for 3 minutes using 4 mW/cm^2 long wave A (UVA) light. After polymerization, the models were cultured in RPMI-1640 with 10% (v/v) fetal bovine serum, 1% (v/v) L-glutamine, and 1% (v/v) penicillin streptomycin for 1 or 7 days.

On days 1 and 7 of culture, DiI labeled control (mRFP) or PRDX1 overexpressing (PRDX1-mRFP) NK-92MI cells were incubated with the 3D culture systems at a 2:1 E:T-cell ratio in RPMI-1640 with 10% (v/v) fetal bovine serum, 1% (v/v) L-glutamine, and 1% (v/v) penicillin–streptomycin on a shaker. After two hours of coculture, the media were removed, the 3D models were rinsed in PBS, and fixed in 10% neutral buffered formalin. The 3D models were moved to a glass dish and imaged with confocal microscopy (Zeiss LSM 880, Carl Zeiss). The images were evaluated for NK cell and cancer cell fluorescent intensity and extent of colocalization of NK cells with cancer cells by the Mander's overlap coefficient (24) using Fiji (NIH).

Lentiviral transduction

For lentiviral transduction, either the standard calcium phosphate method or a polyethyleneimine (PEI) transfection protocol were used. Briefly, 2.6×10^6 HEK293T cells were seeded onto a 10-cm tissue culture dish. The next day, the cells were cotransfected with 8.6 μg of a plasmid containing the gene of interest (SFFV-PRDX1-mRFP, pSEW-CAR-PD-L1, pSLIEW-luc-GFP, or lentiCRISPRv2-sgPDL1), 8.6 μg psPAX2 packaging vector (cat. no. 12260, Addgene), and 5.5 μg pMD2.G envelope vector (cat. no. 12259, Addgene). 48 hours post-transfection, the lentivirus-containing medium was collected, filtrated through a 0.45-μm filter, and centrifuged overnight at 3,500 × *g* at 4°C. The next day, target cells were transduced with the concentrated lentivirus-containing medium. For transfection, target NK-92 and NK-92MI cell lines were resuspended in X-VIVO 20 medium with 5% human serum and IL2 (200 U/mL) supplemented with protamine sulfate (final concentration 15 μg/mL) and BX795 inhibitor (final concentration 6 μmol/L). Cells (2.5×10^5) were transferred to a 50 or 15 mL Falcon tube, and concentrated viral supernatant was added to the cell suspension. The cells with the lentivirus were centrifuged for 1 hour at 750 × *g* at 32°C, then transferred to a 24-well plate and incubated for 24 hours. The next day, all procedures were repeated with a new portion of lentiviral supernatant.

Statistical analysis

Statistical analysis was performed with GraphPad Prism 7 (GraphPad Software). For paired sample sizes $n \geq 5$, statistical analysis was done using the Wilcoxon test. For unpaired samples ($n \geq 5$), the Mann–Whitney test or unpaired *t* test were used. For statistical comparison between more than two groups, two-way ANOVA with *post hoc* analysis was used. For RNA-sequencing (RNA-seq) data, statistical comparison between groups was done with one-way ANOVA. Particular group means were compared using unpaired *t* test. Data were considered significant when *, $P < 0.05$; **, $P < 0.01$; ***, $P < 0.001$; ****, $P < 0.0001$. Only statistically significant differences were marked on the graphs. For low sample sizes $n < 5$, individual data points depict technical replicates, particular measurements, or averages of two technical replicates. Statistical tests are described in detail in figure legends.

RNA-seq data

Public RNA-seq data from four experiments (E-GEOD-60424, E-GEOD-83808, E-GEOD-83115, and E-GEOD-62920) involving either B, T, or NK cells from healthy donors were analyzed. In the case of the E-GEOD-60424 data set, all selected samples had data for all the above-mentioned cell types, whereas E-GEOD-83808 RNA-seq analysis was performed for three healthy patients and involved various subpopulations of T cells, E-GEOD-83115 collected data for B cells and T cells from a single patient (with replicates obtained by sequencing samples at two independent sites), and E-GEOD-62920 included gene-expression for T cells from a single individual. Experiment IDs, as well as cell types and sample IDs are provided in Supplementary Table S1. Read quality was assessed with FastQC (ref. 25; version 0.11.9). Sickle (version 1.33) was used to trim reads fragments with an average quality below 30 in Phred scale and to filter out reads shorter than 40 bp. Processed reads were mapped onto the human GRCh38 reference genome (downloaded from the UCSC database) using STAR (ref. 26;

version 2.7.3a). Samtools (ref. 27; version 1.9) was used to keep only reads with flags 99, 147, 83, or 163 and mapping quality 255. Reads associated with human genes, as defined in the Gencode GTF annotation file V29, were selected using featureCounts function from the RSubRead package (ref. 28; version 1.6.4). As the aggregated data come from different experiments and sequencing platforms, to remove batch effects ComBat from SVA package (29) was used (version 3.34). In downstream analyses, samples were divided into three groups: B, T, and NK cells, even if additional information allowed them to be assigned to a more specific subpopulation of cells. All plots were prepared using the ggplot2 package (ref. 30; version 3.3). R script, phenotype file required by ComBat and text file with commands used in this analysis are available at https://github.com/michallaz/RNASeq_immunnology.

Polysome RNA-seq data of NK cells stimulated with IL15 and IL2

Public RNA-seq data (GSE77808) from six donors were analyzed. For each donor, four polysome mRNA samples of stimulated NK cells were analyzed: (i) IL2 activated, (ii) IL2 activated followed by withdrawal after 48 hours, (iii) IL15 activated, and (iv) IL15 activated followed by withdrawal after 48 hours. Due to low quality of RNA obtained for some samples, Donor 3 contains activation and withdrawal data pooled from two different donors. Read quality was assessed with FastQC. Reads were mapped onto the human GRCh38 reference genome (downloaded from the UCSC database) using STAR (ref. 26; version 2.7.3a). Filtering properly and uniquely mapped reads (with flags 99, 147, 83, or 163) was done using Samtools (27). Exonic gene expression for human genes annotated in the Gencode GTF annotation file V35 was calculated using HTSeq-count (31). Raw gene counts were normalized using TMM method implemented in edgeR package (32, 33) and the final expression was calculated as Counts Per Million (CPM). R script and text file with commands used in this analysis are available at https://github.com/michallaz/RNASeq_immunnology.

Results

Tumors are characterized by increased ROS and redox imbalance

Although elevated ROS are described as a characteristic element of cancer, there are limited data on concentrations of H_2O_2 within the TME. Therefore, we measured H_2O_2 concentrations in breast cancer TIF, a fluid phase representing the tissue microenvironment. Semipermeable membranes were implanted within the tumor masses of subcutaneous 4T1, EMT6, or EO771 murine syngeneic breast cancer models, and then by *in vivo* ultrafiltration, extracellular fluid bathing the tumor, stroma, and immune cells was extracted. The concentrations of H_2O_2 measured in the TIF reached approximately 10 μmol/L in all three tested cell lines, whereas in control fluids isolated either from peripheral blood or subcutaneously implanted membranes (SCF), H_2O_2 was present in undetectable or significantly lower amounts (**Fig. 1**). Immunophenotyping of the 4T1 tumors revealed $CD45^+$ immune cell infiltration into the tumor site, with a dominant population of immature myeloid cells (Supplementary Fig. S1A and S1B), which has been shown to be a cellular source of ROS in the immunosuppressive microenvironment of the tumor (12). We concluded that effector immune cells are exposed to elevated H_2O_2 in tumor tissue fluids upon infiltration into the tumor site.

NK cells are particularly susceptible to oxidative stress

We next determined the sensitivity of different lymphocyte subpopulations to redox stress induced by H_2O_2. We isolated human primary NK, T, and B cells from peripheral blood of healthy donors, incubated them with increasing concentrations of hydrogen peroxide (H_2O_2) or glucose oxidase (GOX) and determined cell viability with PI staining. GOX was used as an enzyme that generates H_2O_2 by oxidation of glucose to D-glucono-δ-lactone. First, to estimate the GOX doses that generate H_2O_2 concentrations similar to those observed *in vivo*, we measured H_2O_2 produced by GOX in the culture medium *in vitro*. We observed that GOX within a range of 0.25–0.5 mU/mL produced approximately 10 μmol/L H_2O_2 (**Fig. 2A**), and therefore these concentrations of GOX were used in our subsequent experiments.

We observed that among lymphocytes isolated from several healthy donors, NK cells are the most sensitive to H_2O_2 and GOX compared with T cells and B cells (**Fig. 2B** and **C**). Significant differences between populations were observed in concentrations as low as 0.125 mU/mL GOX and 6.25 μmol/L of H_2O_2, which correspond to concentrations achievable in murine tumors models *in vivo*. Consistent with previous reports, we also observed that $CD56^{bright}$ cells were more resistant to redox stress in comparison with $CD56^{dim}$ NK cells (Supplementary Fig. S1C; ref. 18). Correspondingly, sodium L-ascorbate (L-ASC), previously demonstrated to generate H_2O_2 in serum-containing culture medium (34), exerted the most pronounced cytotoxic effect against NK cells compared with T and B cells (**Fig. 2D**). Moreover, L-dehydro-ascorbate (L-DHA), an oxidized form of L-ASC that does not generate H_2O_2, was not toxic to NK cells (**Fig. 2E**). Cells were then treated with increasing concentrations of H_2O_2, GOX, and L-ASC in the presence of catalase (CAT), an H_2O_2 scavenger, and their toxicity was entirely reversed by incubation with CAT (**Fig. 2F–H**), further confirming the dominant role of H_2O_2 in the induction of cell death.

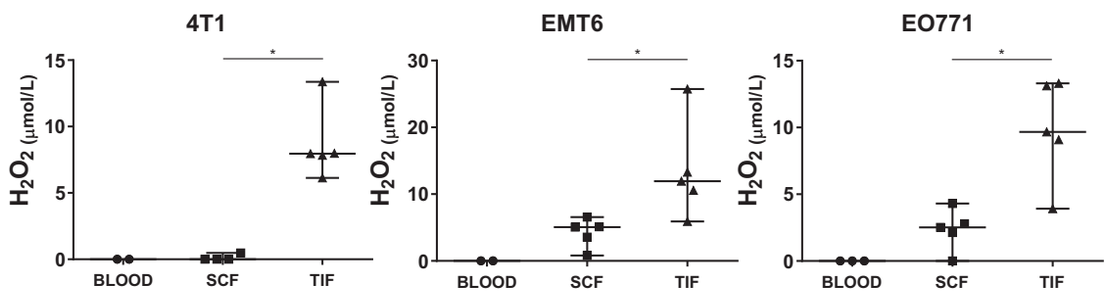

Figure 1.

Detection of H_2O_2 in the TME. H_2O_2 concentrations in blood, subcutaneous fluid (SCF), and TIF collected via ultrafiltration from 4T1, EMT6, and EO771 tumors. Bars represent median with range; dots represent individual mice, $n = 4$–5 (SCF and TIF), $n = 2$–3 (blood). Statistic: Mann–Whitney test.

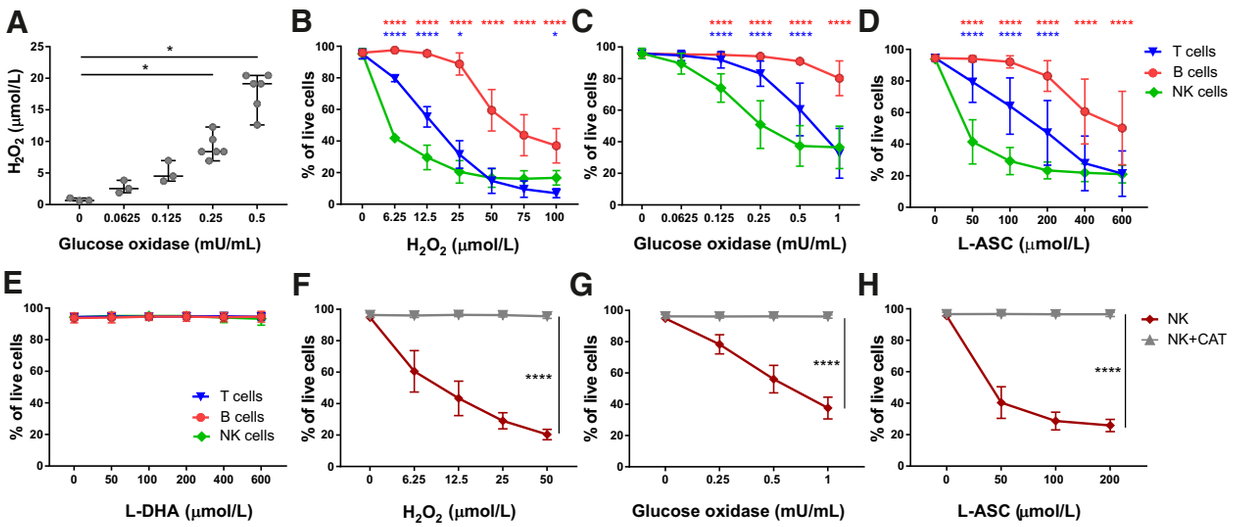

Figure 2.

The sensitivity of human primary T, B, and NK cells to oxidative stress. **A,** H_2O_2 generated by GOX after 4 hours ($n = 3$–6). Bars represent median with range, dots represent average of two technical replicates. Statistic: Mann–Whitney test. **B–E,** Survival of T, B and NK cells after 16 hour-incubation with H_2O_2 (**B**; $n = 7$), GOX (**C**; $n = 5$), sodium ascorbate (**D**; $n = 8$), and L-dehydroascorbate (**E**; $n = 7$), measured by viability staining and flow cytometry. Data shown as mean ± SD. Statistic: two-way ANOVA ($P < 0.0001$), followed by Dunnett *post hoc* test in comparison with NK cells. Statistically significant differences between NK cells and B cells (red stars), and NK cells and T cells (blue stars). **F–H,** NK cell survival after 16 hours of incubation with H_2O_2 (**F**), GOX (**G**), and sodium ascorbate (**H**) in the presence/absence of CAT ($n = 3$). Data shown as mean ± SD; $n = 3$. Statistic: two-way ANOVA, $P < 0.0001$.

Redox stress impairs the cytotoxic activity of NK cells

To investigate how redox stress influences NK cells' functions, we isolated NK cells from peripheral blood of healthy donors and incubated them with increasing concentrations of GOX. The potential of NK cells to kill target tumor cells was assessed by the RTCA, an impedance-based technology used for label-free and real-time monitoring of cytotoxicity. We observed that GOX impairs the ability of NK cells to kill target K562 cells via the natural cytotoxicity mechanism in a dose-dependent manner (**Fig. 3A**), as well as in the ADCC mechanism induced by trastuzumab against HER2-positive MCF-7 (**Fig. 3B**) and SK-BR-3 cell lines (Supplementary Fig. S2). We confirmed NK-mediated ADCC in the absence of trastuzumab for both MCF-7 (Supplementary Fig. S3A) and SK-BR3 (Supplementary Fig. S3B) cell lines. Altogether, these results provided direct evidence that redox stress induced by H_2O_2 impairs the antitumor activity of NK cells.

The scavenging potential of thiols and H_2O_2 transport ability does not explain the high susceptibility of NK cells to redox stress

To further explore the molecular basis for the high sensitivity of NK cells to redox stress, we performed experiments determining the H_2O_2 transport capability and antioxidative capacity of T, B, and NK cells. We determined the concentrations of both extracellular and intracellular free thiols to estimate the H_2O_2 scavenging potential of lymphocytes. Extracellular cell-surface-free thiols (CSFT) in T, B, and NK cells were analyzed by staining with the maleimide derivative of Alexa Fluor 647 dye. We observed the highest level of CSFT in B cells, whereas T cells and NK cells were characterized by lower CSFT (Supplementary Fig. S4A). Within the NK cell population, we observed increased CSFT in the $CD56^{bright}$ subpopulation, comparable with those observed in B cells and significantly higher than in $CD56^{dim}$ cells (Supplementary Fig. S4B), which was in accordance with a previous study (18). Furthermore, with ThiolTracker Violet probe, we found that reduced GSH, representing the majority of intracellular free thiols, was the highest in NK cells when compared with T and B cells (Supplementary Fig. S4C). This does not, however, explain the sensitivity of NK cells to redox stress. Therefore, we compared the H_2O_2 transport capacity between the selected lymphocyte subpopulations. Although H_2O_2 has been long believed to cross cell membranes freely, several recent studies point out that mammalian membranes are relatively poorly permeable to H_2O_2 (6, 35). Today, it is widely accepted that aquaporins promote the transport of water and H_2O_2 as diffusion-facilitating channel proteins (6). To determine the expression of various aquaporins in different lymphocyte subsets, we performed RNA-seq analysis of publicly available data (Supplementary Table S1). In our analysis of T, B, and NK cells, we only detected the expression of *AQP3* and *AQP11*; however, *AQP11* expression was very low (Supplementary Fig. S4D). *AQP3* expression, although similar in both B cells and NK cells, was significantly higher in T cells (Supplementary Fig. S4D). We further confirmed these findings by qRT-PCR in lymphocytes isolated from healthy donors (Supplementary Fig. S4E). In summary, these data show that the high susceptibility of NK cells to redox stress is not the result of low extra/intracellular free thiol scavenging activity or increased ability to transport H_2O_2 through the membrane.

We next assessed ROS concentrations in T, B, and NK cells, at steady state and in response to H_2O_2. We observed similar CM-H_2-DCFDA staining in NK, T, and B cells, which was further increased upon incubation with H_2O_2 (Supplementary Fig. S4F). Although CM-H_2-DCFDA is the most widely used probe for detecting intracellular ROS, CM-H_2-DCFDA is a thiol-reactive probe, and its fluorescence cannot be used as a direct measure of H_2O_2 (36). Therefore, we also performed stainings with CellROX Reagents, namely, CellROX Deep Red, for ROS localized primarily in the cytoplasm and mitochondria, and CellROX Green, a nucleic acid

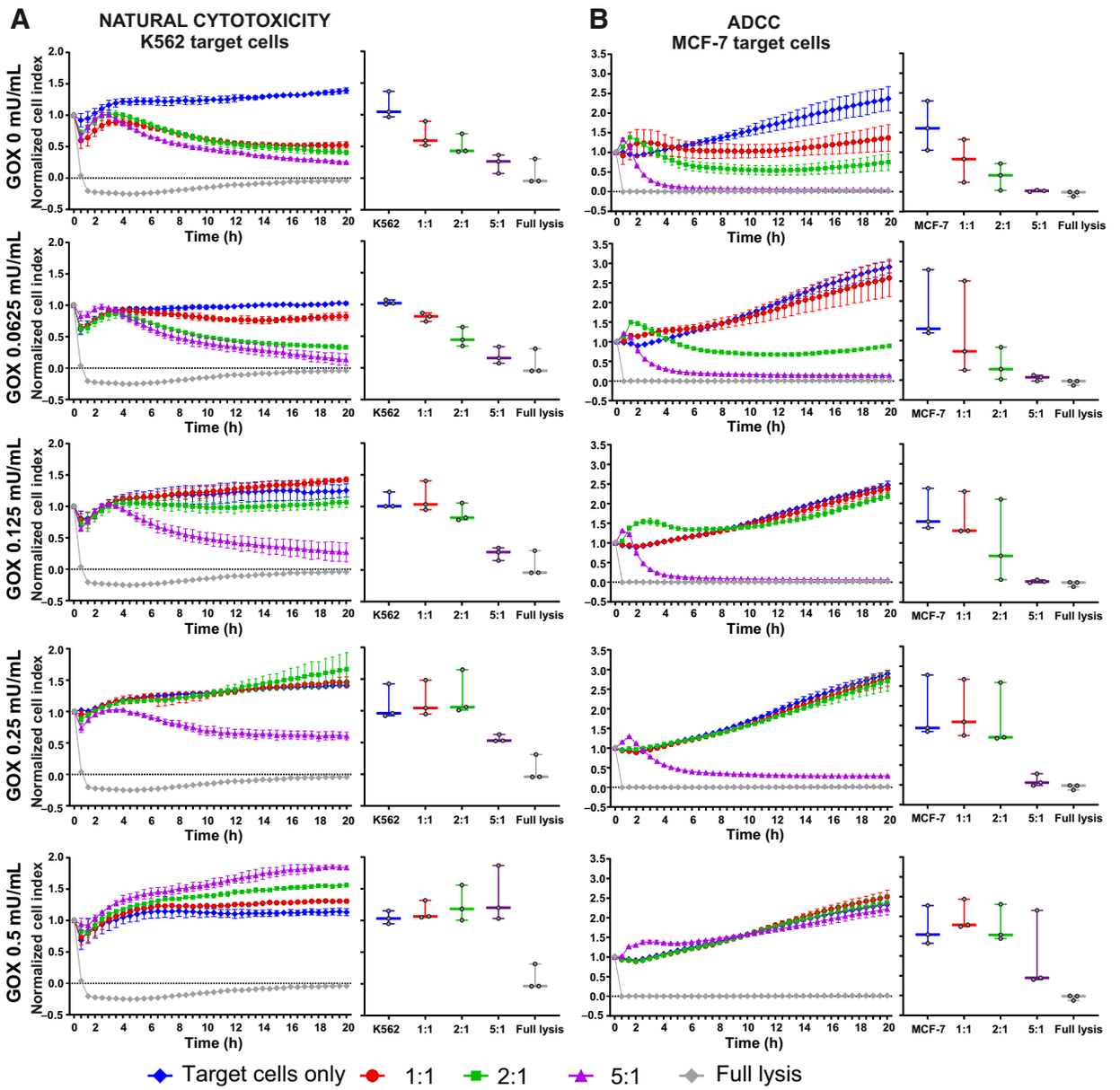

Figure 3.

RTCA analysis of resting human primary NK cell cytotoxicity in the oxidative stress conditions generated by GOX. Natural cytotoxicity of human primary NK cells toward K562 targets (**A**) or trastuzumab-dependent cell-mediated cytotoxicity of human primary NK cells against MCF-7 targets (**B**; E:T ratio 1:1, 2:1, 5:1) as measured by RTCA. Left, representative experiment from one donor. Data shown as averages ± SD from two technical replicates. Right, data of three independent experiments (19 hours after the effectors' addition) presented as median with range. Dots represent average of two technical replicates.

binding dye, for ROS localized in the nucleus (37). Consistent with previous observations (38), $CD56^{bright}$ cells accumulated less ROS when compared with $CD56^{dim}$ cells, as determined by CellROX Deep Red (Supplementary Fig. S4G). However, in comparison with T and B cells, bulk NK cells were characterized by the lowest basal cytoplasmic ROS concentration (Supplementary Fig. S4H) and comparable nuclear ROS concentration (Supplementary Fig. S4I). Nonetheless, upon incubation with H_2O_2, the most pronounced changes in ROS accumulation were detected in NK cells (Supplementary Fig. S4H and S4I). Both B cells and T cells efficiently endured the conditions of oxidative stress, as illustrated by relatively small changes in ROS accumulation upon the treatment with H_2O_2.

We concluded that NK cells, although rich in intracellular thiols, do not efficiently mitigate oxidative stress and do not have the potential to scavenge accumulating ROS. H_2O_2, as a relatively stable molecule, reacts very slowly with glutathione and other thiols (39). Upon a buildup of ROS in a cell, enzymatic antioxidants play a more important role in fast neutralization and detoxification of excessive ROS (7, 40). Therefore, we subsequently analyzed the expression of antioxidant enzymes that play the role of cellular sinks for H_2O_2.

NK cells lowly express select intracellular antioxidative enzymes

To investigate T, B, and NK cells for intracellular antioxidative capacity, we determined the abundance of enzymes involved in maintaining redox homeostasis. Within the cells, superoxide dismutases catalyze the conversion of $O_2^{\bullet-}$ into H_2O_2 and O_2. H_2O_2 is further eliminated by CAT or by thiol peroxidases, such as GPXs and PRDXs (**Fig. 4A**; ref. 41). Therefore, in our study, we analyzed publicly available transcriptomic data of unstimulated primary NK, T, and B cells for select enzymes of intracellular redox homeostasis. The analysis comprised the superoxide dismutases (SOD), CAT, GPXs, PRDXs, and the enzymes involved in restoring their reduced state (thioredoxins and thioredoxin reductases), as well as enzymes involved in glutathione metabolism (glutathione reductase and glutaredoxin). Many of the analyzed enzymes were differentially expressed between NK and T cells or NK and B cells (**Fig. 4A**; Supplementary Fig. S5A), but the expression of only two enzymes (*PRDX1* and *GPX1*) was significantly lower in NK cells, when compared with both T cells and B cells (**Fig. 4A**). For every individual donor, we observed the same trend of the lowest expression of *PRDX1* and *GPX1* in NK cells when compared with T and B cells (Supplementary Fig. S5B). The expression pattern of SOD1, CAT, as well as enzymes of both thioredoxin system (TXN1, TXNRD1) and glutathione system (GSR), was further confirmed by qRT-PCR and WB experiments (**Fig. 4B–D**; Supplementary Fig. S5C and S5D). However, in qRT-PCR (**Fig. 4B**) and WB analyses (**Fig. 4C** and **D**; Supplementary Fig. S5D), we confirmed that only PRDX1 expression is consistently the lowest in NK cells compared with T and B cells. GPX1 expression, although more heterogeneous and donor-dependent than other analyzed enzymes, was in NK cells more similar to that observed in T cells. We also observed significant differences between $CD56^{bright}$ and $CD56^{dim}$ cells, with increased expression of all analyzed enzymes, including PRDX1, in the $CD56^{bright}$ subpopulation, as compared with the $CD56^{dim}$ subpopulation (Supplementary Fig. S5E and S5F). These findings further support and help explain the phenomenon of the relatively high resistance of $CD56^{bright}$ cells to oxidative stress. We hypothesized that the high sensitivity of NK cells to redox stress is a result of their intrinsically low expression of PRDX1, an essential component of the PRDX/TXN/TXNRD system, and subsequent low intracellular antioxidative potential.

Priming with IL15 increases NK cell tolerance of redox stress and the expression of the PRDX/TXN/TXNRD system

It has already been documented that IL15, a cytokine necessary for NK cell development and effector activity, supports the persistence of infused NK cells (42) and increases their resistance to oxidative stress (38). We confirmed that priming with IL15 increases NK cell tolerance to redox stress by assessing cytoxicity at various GOX concentrations (**Fig. 5A** and **B**). To identify the transcriptional program associated with increased NK cell resistance against oxidative stress, we analyzed single-cell transcriptomes of resting and proliferating NK cell subsets upon treatment with IL15 (43). Briefly, we sorted and sequenced less-differentiated $CD56^{dim}$ $NKG2A^+KIR^-$ NK cells and more differentiated $NKG2A^-KIR^+$ at baseline and after IL15 stimulation for 6 days. At the end of the experiment, we sorted the mature KIR^+ NK cells into slowly and rapidly cycling cells before RNA-seq. For *PRDX1* (**Fig. 5C**), as well as *TXN1*, *TXNRD1*, and thioredoxin-interacting protein (*TXNIP*; Supplementary Fig. S6A), we observed increased expression and an increase in the proportions of cells expressing these genes in the IL15-stimulated cells compared with the cells at baseline. This increase was even more robust in rapidly cycling (generation 2+) KIR^+ cells.

We further verified the results of our RNA-seq analysis by WB and qRT-PCR in NK cells isolated from healthy donors. We discovered a significant upregulation of PRDX1 at both protein (**Fig. 5D**) and mRNA (**Fig. 5E**) levels already after 24 hours of treatment of NK cells with IL15. This increase was accompanied by the upregulation of *TXN1* and *TXNRD1* (Supplementary Fig. S6B). Interestingly, upregulation of thioredoxin system–related enzymes appeared to be a more general phenomenon triggered by various stimuli and observed in different lymphocyte subpopulations. Specifically, we detected an increase of PRDX1/TXN1/TXNRD1 at both mRNA and protein levels in NK cells stimulated with anti-CD2/NKp46 (Supplementary Fig. S6C and S6D), in T cells stimulated with IL2 and anti-CD3/CD28 beads (Supplementary Fig. S6E and S6F), and in B cells activated by CD40L-expressing feeder cells (Supplementary Fig. S6G). Furthermore, we observed that IL15 stimulated the expression of *PRDX1* and the thioredoxin system in an mTOR-dependent manner, as the mTOR inhibitor Torin 1 prevented the IL15-induced increase of *PRDX1/TXN1/TXNRD1* in primary NK cells (**Fig. 5F**) and the NK-92 cell line (Supplementary Fig. S6H). By reanalyzing the publicly available translatome (polysome-associated RNA) data of NK cells from five donors stimulated with IL2 or IL15 (44), we further confirmed the results of Yang and colleagues, who observed upregulation of TXN1 and reduced expression of its inhibitor (TXNIP) upon treatment with IL15, as compared with IL2 (Supplementary Fig. S6I; ref. 38). However, in polysome-associated mRNA of IL15 primed NK cells, we additionally noted increasing PRDX1 expression (Supplementary Fig. S6I).

Altogether, our results demonstrate that IL15 enhances NK cells' resistance against oxidative stress by upregulating the PRDX/TXN/TXNRD system. However, post-cytokine activation conditions should be considered for the clinical context of NK cell–based immunotherapies. It has been shown that IL15 not only directly changes gene expression but also primes NK cells to respond to cytokine withdrawal via augmented mTOR signaling and an IL15-primed gene-expression program (3, 44). Here, after IL15 withdrawal, we already observed a significant downregulation of *PRDX1* expression (**Fig. 5G**), accompanied by the decrease of *TXN1* and *TXNRD1* (Supplementary Fig. S6J). Subsequently, we further confirmed our findings by the reanalysis of RNA-seq data, where we also detected downregulation of PRDX1 and TXN1/TXNRD1 in polysome-associated mRNA fraction upon IL15 withdrawal (Supplementary Fig. S6I). We therefore found the effects of IL15 on the expression of select antioxidant enzymes to be transient and strictly dependent on the presence of the cytokine.

PRDX1 overexpression improves the viability of NK cells under H_2O_2-induced oxidative stress

With our understanding of the role of the PRDX/TXN/TXNRD pathway in NK cell redox stress, we sought to modify NK cells to promote a durable response under those conditions. First, we electroporated IL15-treated NK cells isolated from healthy donors with the transcribed *in vitro* PRDX1 mRNA (**Fig. 6A**, left; Supplementary Fig. S7A). In accordance with our previous results, we noticed an increase of *PRDX1* expression upon IL15 priming that was further potentiated by electroporation of PRDX1 mRNA. To examine whether PRDX1-modified NK cells were more resistant to oxidative stress, cells were cultured with GOX and checked for viability (**Fig. 6B** and **C**). The most pronounced differences between the viability of PRDX1 NK and mock-transfected NK cells were observed for 0.5 and 1 mU/mL GOX (**Fig. 6B** and **C**).

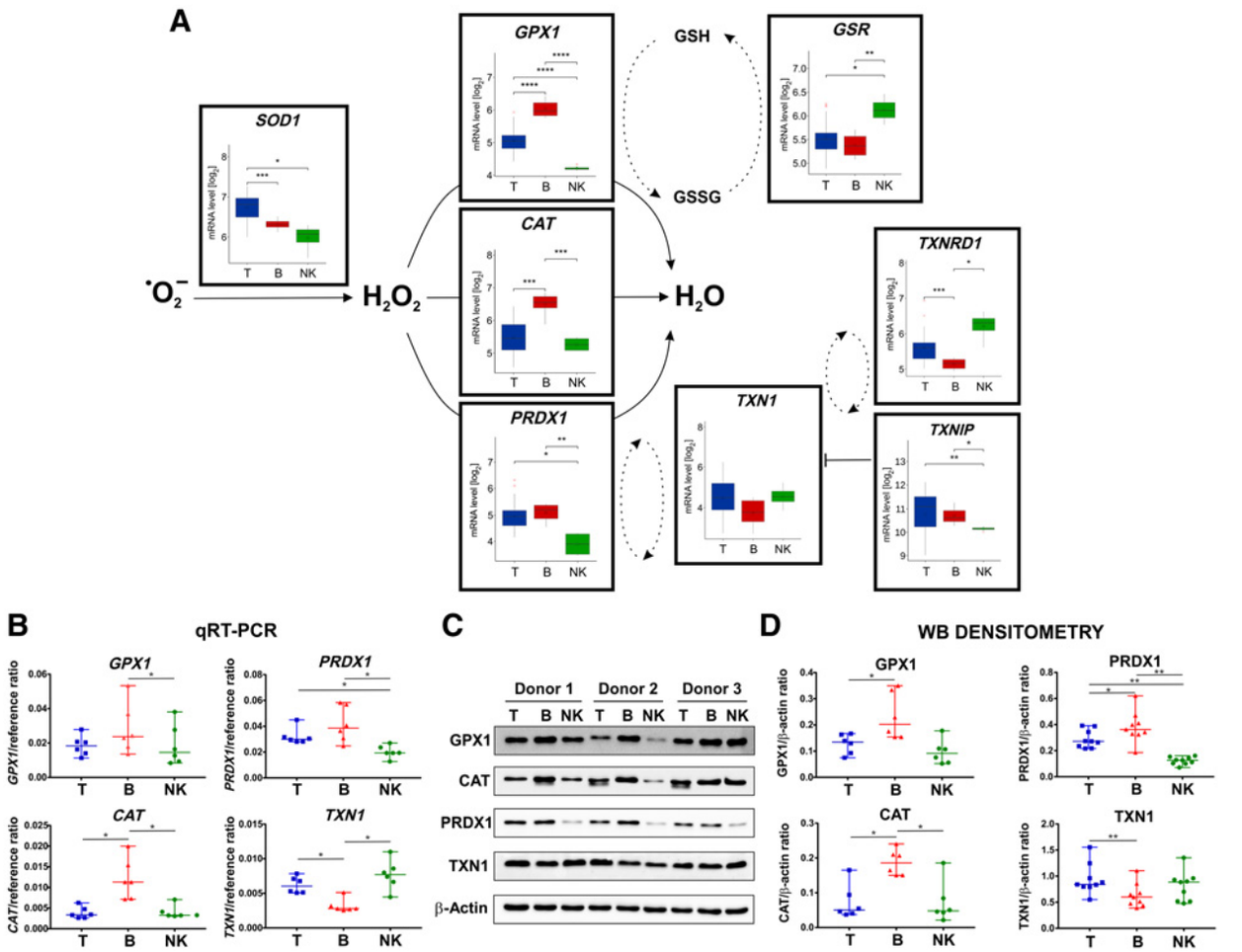

Figure 4.

Expression of select antioxidant enzymes in human primary T, B, and NK cells. **A,** Analysis of publicly available RNA-seq data for select antioxidant enzymes in nonstimulated human primary T ($n = 26$), B ($n = 11$), and NK cells ($n = 4$). Statistical significance determined by one-way ANOVA. Unpaired *t* test used for comparisons between groups. Log2 CPM expression of particular antioxidant enzymes shown as average gene expression and median. Outlier samples shown as red crosses. **B,** qRT-PCR analysis of select antioxidant enzymes in human nonstimulated T, B and NK cells ($n = 6$ donors). Data shown as median and range. Points show average of two technical replicates. Statistic: Wilcoxon test. **C,** Representative Western blot analysis of GPX1, CAT, PRDX1, TXN1, and β-actin level of human primary T, B, and NK cells from three independent donors. **D,** Densitometry analysis of GPX1 ($n = 6$), CAT ($n = 6$), PRDX1 ($n = 9$), and TXN1 ($n = 9$) expression calculated as ratio to β-actin loading control. Statistic: Wilcoxon test.

Because NK-92 cells are used for adoptive therapy in patients, we used lentiviral transduction to overexpress PRDX1 in NK-92MI cells, as demonstrated by WB analysis (**Fig. 6A**, right). We observed that NK-92MI cells were less sensitive to H_2O_2-induced oxidative stress because 0.5 mU/mL GOX affected their viability to a lesser extent compared with primary NK cells (**Fig. 6C** and **E**). Nonetheless, at 1 mU/mL GOX, only 30% of control NK-92MI cells were alive, whereas PRDX1-NK-92MI cells retained higher viability, ranging from around 55% to 90% (**Fig. 6E**, left). From these experiments, we concluded that engineering both primary NK cells and NK-92 cells to overexpress PRDX1 is a feasible approach to support NK cell viability under oxidative stress.

PRDX1 overexpression improves the viability and function of CAR-endowed NK cells under H_2O_2-induced oxidative stress

NK cell modification with CARs is becoming an alternative therapeutic option to CAR T cells for cancer immunotherapy. Therefore, in our study we next asked whether CAR-expressing NK-92 cells maintain their antitumor activity under oxidative stress. As a proof-of-concept model, we modified both primary NK and NK-92MI cells with CD19 CAR (FMC-63) and/or PRDX1 mRNA. The modification efficiency of cells with CAR was checked by flow cytometry (Supplementary Fig. S7B and S7C). Primary and NK-92MI cells modified to express PRDX1, both control (mRFP MOCK and PRDX1-mRFP MOCK) and expressing CD19 CAR (mRFP CAR-CD19 and PRDX1-mRFP CAR-CD19), were substantially protected from oxidative stress induced by increasing concentrations of GOX-generated H_2O_2 (Supplementary Fig. S7D–S7F).

It has been shown that oxidative stress plays an important role in breast cancer and is most often associated with an aggressive phenotype (45). We also confirmed these observations by measuring H_2O_2 concentrations in *in vivo* breast cancer model (**Fig. 1**). Thus, we targeted triple-negative breast cancer PD-L1–expressing MDA-MB-231 cells with PD-L1–directed atezolizumab-based CAR NK cells.

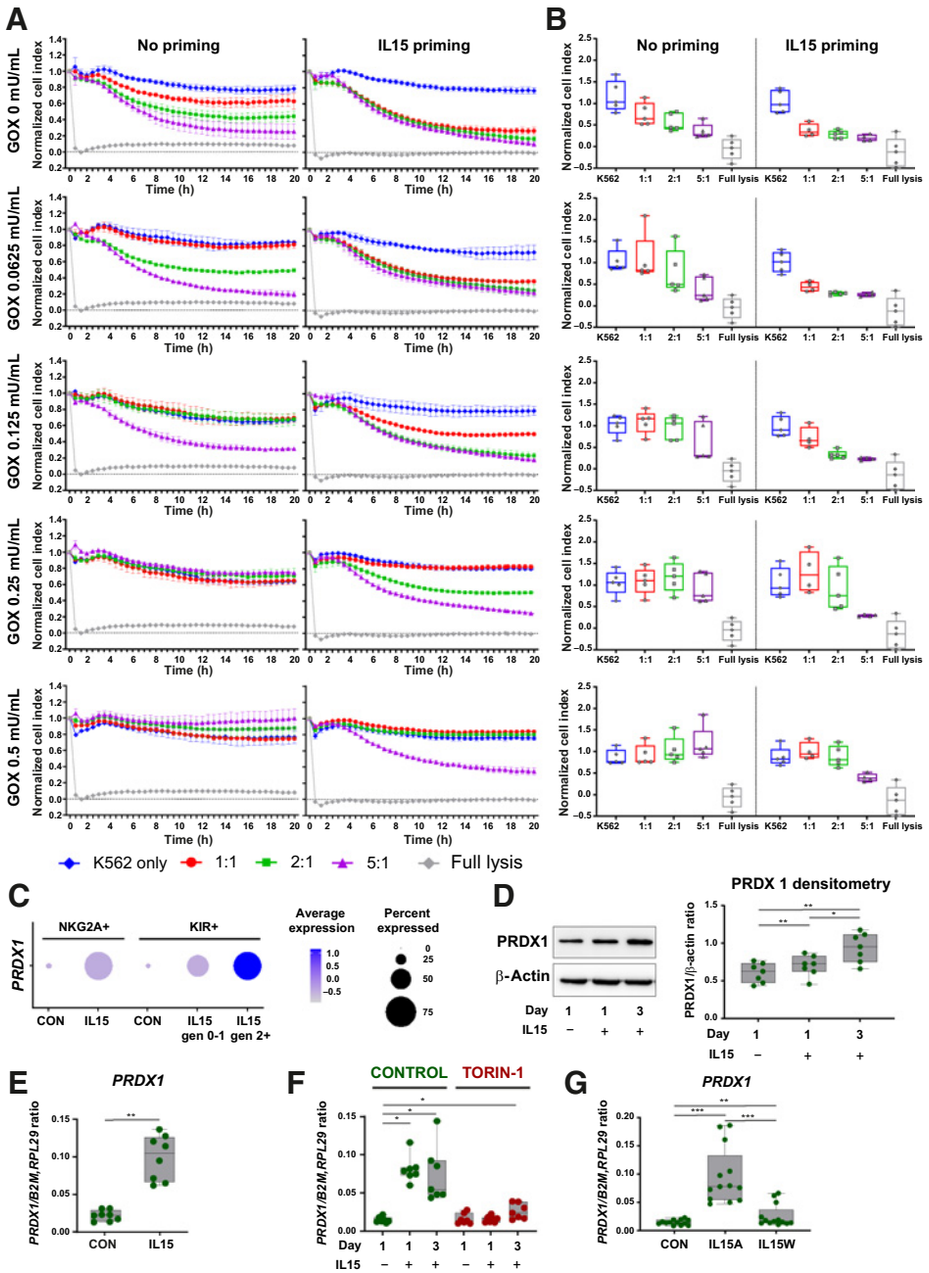

Figure 5.

Influence of NK cell priming with IL15 on the natural cytotoxicity and the expression of select antioxidant enzymes. **A,** Representative RTCA cytotoxicity of nonstimulated (left) and IL15-stimulated (right) NK cells toward K562 targets in the presence of increasing concentrations of GOX (E:T ratios: 1:1, 2:1, 5:1). Data show averages ± SD from two technical replicates. **B,** Summary of RTCA cytotoxicity experiments ($n = 5$) at 19 hours after effectors' addition. Left: nonstimulated; right: IL15-stimulated NK cells. Data show median with range. Dots represent average of two technical replicates. **C,** scRNA-seq analysis of *PRDX1* in different NK cell subsets stimulated with IL15. The scRNA-seq data were processed using Seurat 3. Samples within each subset were merged, and the dot plot shows for each gene the average expression level in the subsets as well as the percentage of cells within the subsets that expressed the gene. Visualization was generated using the DotPlot function within the Seurat toolkit. **D,** Western blot analysis of PRDX1 in nonstimulated and IL15-stimulated (10 ng/mL) NK cells. Left: representative blot from one donor; right: densitometry analysis of PRDX1/β-actin ratio ($n = 7$ donors). Data shown as median and range. Dots represent individual donors. Statistic: Wilcoxon test. **E,** qRT-PCR analysis of *PRDX1* in nonstimulated and IL15-stimulated NK cells (10 ng/mL, 24 hours). Data show median and range. ($n = 8$ donors). Dots represent the average of two technical replicates. Statistic: Wilcoxon test. **F,** qRT-PCR analysis of *PRDX1* after mTOR inhibition with Torin 1 (1 μmol/L) in nonstimulated and IL15-stimulated NK cells (10 ng/mL). Data show median and range ($n = 7$ donors). Dots represent the average from two technical replicates. Statistic: Wilcoxon test, in comparison with control nonstimulated group. **G,** qRT-PCR analysis of *PRDX1* in nonstimulated NK cells (CON), after IL15 stimulation (10 ng/mL, 48 hours; IL15A) and IL15 stimulation (48 hours) followed by cytokine withdrawal (24 hours) (IL15W). Data show median and range ($n = 13$ donors). Dots represent the average from two technical replicates. Statistic: Wilcoxon test.

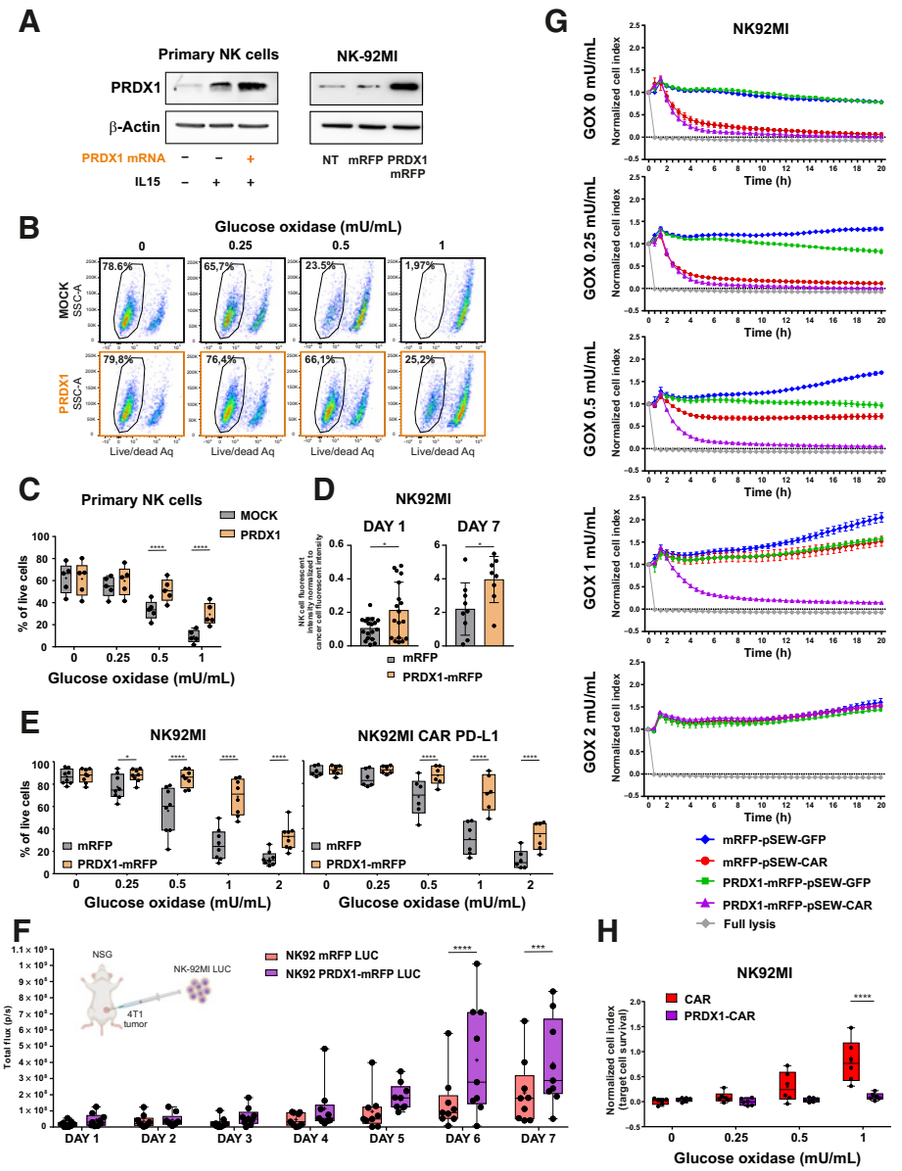

Figure 6.

PRDX1 overexpression in primary NK cells and CAR-PD-L1 NK-92MI improves survival and cytotoxicity in oxidative stress. **A,** Western blotting analysis of PRDX1 in primary NK cells (left) and NK-92MI cell line (right). Primary NK cells (representative donor) were nonstimulated or IL15-stimulated (10 ng/mL, 3 days), and electroporated with *in vitro* transcribed PRDX1 mRNA or not. NK-92MI cell line was nontransduced (NT) or transduced with control (SFFV-IRES-mRFP) and PRDX1-encoding plasmid (SFFV-PRDX1-IRES-mRFP). **B,** Representative dot plots (flow cytometry) of control (MOCK) and PRDX1-mRNA electroporated NK cells incubated with GOX. **C,** Viability of MOCK and PRDX1-mRNA electroporated human primary NK cells in the presence of GOX assessed by flow cytometry ($n = 5$). Data points show the average from two technical replicates with median (horizontal line) and mean (plus symbol). Statistic: two-way ANOVA ($P = 0.0002$) with Bonferroni *post hoc*. **D,** Migration of mRFP-NK-92MI and NK-92MI-PRDX1 cell lines into an engineered 3D hydrogel scaffold on day 1 (left) or day 7 (right), determined by fluorescence intensity of NK cells normalized to cancer cell fluorescent intensity. Left: $n = 18$ in both mRFP and PRDX1-mRFP group. Right: $n = 9$ (mRFP), $n = 8$ (PRDX1-mRFP). Data show mean and SD. Statistic: unpaired *t* test. **E,** Survival of NK-92MI-mRFP and NK-92MI-PRDX1-mRFP cell lines (left, $n = 8$) or CAR-PDL-1-NK-92MI cells (mRFP) and CAR-PD-L1-PRDX1-NK-92MI (PRDX1-mRFP) cells (right, $n = 6$) in the presence of GOX (20 hours) assessed with flow cytometry. Data show median (horizontal line) and mean (plus symbol) with range. Dots represent the average from two technical replicates. Statistic: two-way ANOVA ($P < 0.0001$) with Bonferroni *post hoc*. Results of Bonferroni *post hoc* were marked on the graph. **F,** IVIS imaging of the bioluminescence signal of NK-92MI-mRFP-LUC or PRDX1-mRFP-LUC cells administered intratumorally into 4T1 tumors in NSG mice. Data show median (horizontal line) and mean (plus symbol) with range. Points represent bioluminescence signal from each mouse. The experiment was performed twice. All data from two independent experiments were pooled ($n = 9$). Statistic: two-way ANOVA ($P < 0.0001$) with Bonferroni *post hoc*. Bonferroni *post hoc* results were marked on the graph. Intratumoral administration scheme was created with BioRender.com. **G,** RTCA cytotoxicity of CAR-PD-L1-NK-92MI and CAR-PD-L1-PRDX1-NK-92MI cells toward PD-L1+MDA-MB-231 cells in different GOX concentrations (E:T ratio 1:1). Representative results from one experiment. Data shown as averages ± SD from two technical replicates. **H,** Summary RTCA cytotoxicity data ($n = 6$) at 19 hours after effectors' addition. Data shown as median (horizontal line) and mean (plus symbol) with range. Points represent the average of two technical replicates. Statistic: two-way ANOVA ($P < 0.001$) with Bonferroni *post hoc*. Significant differences of Bonferroni *post hoc* were marked on the graph.

First, we stably modified both NK-92MI and PRDX1-NK-92MI cells with the anti–PD-L1 CAR and confirmed its expression by flow cytometry (Supplementary Fig. S7G). We observed that introduction of the CAR into NK-92MI cells did not influence their sensitivity to GOX, as the viability of both control (mRFP-pSEW-GFP; Supplementary Fig. S7H) and CAR-expressing cells (mRFP-pSEW-CAR; **Fig. 6E**, right) dropped to approximately 20%–40% at 1 mU/mL GOX. PRDX1-overexpression increased the viability of both control (mRFP-pSEW-GFP; Supplementary Fig. S7H) and CAR-expressing cells (mRFP-pSEW-CAR) (**Fig. 6E**, right). To further validate human NK-92 PRDX1-overexpressing cells in an *in vivo* settings, we used a xenogeneic NSG murine model inoculated with human breast cancer cells. In contrast to our previous findings in syngeneic breast cancer tumors (**Fig. 1**), the concentrations of H_2O_2 measured in TIF isolated from either MDA-MB-231 or MCF-7 xenogeneic murine model were not significantly different from those detected in SCF (Supplementary Fig. S8A). Therefore, we subsequently used the murine 4T1 cell line inoculated into NSG mice, where we detected high H_2O_2 concentrations in TIF (approximately 30 μmol/L) that significantly exceeded those observed in SCF (Supplementary Fig. S8A). In this model, we intratumorally injected tumor masses with NK-92 cells modified with luciferase (NK92 mRFP LUC) and PRDX1-overexpressing cells (NK92 PRDX1 mRFP LUC) to monitor the survival of NK cells within the tumor for 7 consecutive days. We observed significantly higher bioluminescence of NK92 PRDX1 mRFP LUC cells compared with control NK92 mRFP LUC (**Fig. 6F**). *In vitro* proliferation experiments showed that NK92 PRDX1 mRFP LUC cells proliferated slightly faster than NK92 mRFP LUC cells (Supplementary Fig. S8B). From these experiments, we concluded that PRDX1 overexpression supports both the proliferation of NK-92 cells and their *in vivo* survival in the TME.

To further characterize the influence of PRDX1 on the tumor infiltration of NK cells, we used a 3D hydrogel culture system that recapitulates features of the *in vivo* solid TME and enables visualization and quantification of NK cell migration and interaction with cancer cells (23). In the 3D A549 tumor model, at both 1 and 7 days of culture, we observed a significant increase in migration of NK-92 PRDX1 cells compared with control cells, when quantified as an average NK fluorescence intensity normalized to cancer cells fluorescence intensity (**Fig. 6D**; Supplementary Fig. S8C). At the same time, the Mander's overlap coefficient for colocalization between NK cells and cancer cells was higher for NK-92 PRDX1 cells; however, this trend was not statistically significant (Supplementary Fig. S8D). To further assess the influence of oxidative stress on cytotoxic functions of PD-L1 CAR NK-92MI cells against target MDA-MB-231 tumor cells, we used the RTCA assay (**Fig. 6G**). Specificity of PD-L1 CAR NK-92MI cells was checked against both parental and PD-L1 knockout (sgPD-L1) MDA-MB-231 cells generated by CRISPR-Cas9 knockout (Supplementary Fig. S8E). We observed that sgPD-L1 MDA-MB-231 cells were less efficiently killed by PD-L1 CAR NK-92MI cells when compared with parental MDA-MB-231 cells. However, we observed some residual killing of sgPD-L1 MDA-MB-231 cells, which we attributed to the ability of NK cells to kill in a natural cytotoxicity manner, independently of CAR target expression (Supplementary Fig. S8F). The cytotoxic function of CAR-NK92MI cells was inhibited at 0.5 mU/mL GOX concentration, which did not significantly affect the viability of effector cells, and PRDX1 overexpression provided PD-L1 CAR NK cells with an efficient rescue from the suppressive effects of oxidative stress (**Fig. 6G**). The protective effect of PRDX1 was evident at both 0.5 and 1 mU/mL GOX, representing physiologically relevant H_2O_2 concentrations.

Altogether, our results demonstrate that PRDX1 overexpression is a useful strategy for supporting NK cell functions in immunosuppressive conditions mediated by oxidative stress. Importantly, this strategy provides effector cells with stable expression of PRDX1 independent of IL15. Moreover, PRDX1 overexpression mimics the function of IL15 as a regulator of NK cells' activity in oxidative stress, even in the conditions of cytokine withdrawal.

Discussion

NK cells are currently implemented in extensive clinical trials using autologous and allogeneic NK cell infusion strategies, as well as NK cell lines, including CAR NK (46). Nevertheless, redox imbalance is one of the obstacles to the effective functions of NK cells against solid tumors. Our results provide evidence that redox stress impairs the antitumor activity of NK cells and can contribute to tumor immune evasion from natural NK cell–mediated immune surveillance, as well as to the resistance of tumors to NK cell–dependent immunotherapies.

Others have already demonstrated that increased oxidative stress can promote tumorigenesis (12), tumor progression, and the development of metastasis (47). In breast cancers in particular, oxidative stress has been documented as a driving factor for cancer progression (10). Our study confirmed these observations by quantifying H_2O_2 in a murine breast cancer model *in vivo*. Here we show that the concentrations of H_2O_2 in TIF isolated by ultrafiltration are significantly higher than those observed in blood or subcutaneous fluid isolated from healthy tissue.

The elevated H_2O_2 in breast cancer prompted us to investigate the role of increased ROS in tumor immunosurveillance. We determined the sensitivity of different lymphocyte subpopulations to increasing H_2O_2 concentrations and concluded that NK cells are the most sensitive, and as such, they need to be supported in oxidative stress conditions. These results are in line with previous studies, where NK cells were documented to be more prone to apoptosis induced by monocytes/macrophages-derived ROS than T cells (48). Moreover, two to five times higher concentrations of exogenously added H_2O_2 has been shown to be required to induce apoptosis in T cells compared with NK cells (16). High ROS concentration within the TME has also been shown by others to dampen the antitumor activity of NK cells, both *in vitro* and *in vivo* (49, 50). We confirmed and extended these observations by showing that ROS exerted detrimental effects on NK cell viability and cytotoxicity in various settings. We observed that H_2O_2 compromised the natural cytotoxicity of NK cells and the ability to kill tumor cell by ADCC via trastuzumab, a HER-2–targeting antibody. As dozens of therapeutic antibodies appear to function, in part, through the activation of NK cells (51), and some of these antibodies can also trigger oxidative stress (52), excessive ROS may diminish their efficacy. Furthermore, in the presence of increasing H_2O_2 concentrations, we observed suppressed antitumor activity of CAR NK cells.

Although several groups have studied NK cells' functions under redox stress, the reasons for the high susceptibility of NK cells to ROS are not entirely understood. In previous reports, $CD56^{bright}$ and $CD56^{dim}$ NK cells were compared extensively, and $CD56^{dim}$ cells were reproducibly shown to be highly sensitive to H_2O_2, whereas $CD56^{bright}$ remained largely unaffected (17, 18, 38). In our studies, we confirmed that $CD56^{bright}$ NK cells have higher antioxidative ability and expressed higher quantities of cell-surface thiols than $CD56^{dim}$ NK cells (17, 38). Previously, these observations were explained by higher expression of GPX1 and TXN1 in $CD56^{bright}$ NK cells (18, 38). Our analysis suggests that $CD56^{bright}$ NK cells are characterized by the

higher expression of an array of antioxidant enzymes, including CAT, GPX, PRDX, and TXN/TXNRD, when compared with $CD56^{dim}$ NK cells. This could help explain why $CD56^{bright}$ NK cells accumulate disproportionally at the cost of $CD56^{dim}$ NK cells within tumors (19). Nevertheless, to the best of our knowledge, no comprehensive comparison of the sensitivity to ROS of various lymphocyte populations has been performed so far. Here, we analyzed the key antioxidant systems involved in maintaining a proper redox balance in T, B, and NK cells. Outside the cell, the antioxidant defense system relies on the redox status of extracellular protein thiol groups. However, we observed NK cells were not deficient in extracellular protein thiol groups. Because external H_2O_2 undergoes facilitated and regulated diffusion across organelle and plasma membranes through channel transporters (6), we next determined the expression of AQPs in T, B, and NK cells. AQP3 expression in NK cells was similar to in B cells and significantly lower than in T cells, which also did not explain the high susceptibility of NK cells to oxidative stress. Furthermore, we observed that NK cells were rich in intracellular thiols but had a lower overall antioxidative capacity when compared with T and B cells. Based on the analysis of the expression of a range of antioxidant enzymes, we identified PRDX1 as lacking in NK cells' antioxidant defense system. We determined that modification of NK cells with PRDX1 effectively protected them against oxidative stress.

Higher persistence and expansion of infused NK cells can be important for the overall antitumor efficacy of NK cell–based approaches (53). IL15, currently being tested in several clinical trials, appears to be the most logical choice to enhance the immunotherapeutic effect of NK cells (54, 55). It has been recently shown that IL15-primed NK cells acquire resistance against oxidative stress through thioredoxin upregulation (38). In another study, expansion of NK cells with 4-1BBL and membrane IL15-expressing feeder cells upregulated the expression of both thioredoxin and peroxiredoxin (56). In our study, we confirm these observations; however, we also demonstrate that the effect of IL15 on antioxidative defense is transient, strictly dependent on its presence. Although priming with IL15 was shown to turn on the gene-expression pattern in NK cells and improve the post-cytokine-withdrawal functions, when compared with IL2 (44), we observed that enzymes of the PRDX/TXN/TXNRD system were downregulated upon IL15 withdrawal. The effects of continuous exposure of NK cells to IL15 are also unclear, and it has been recently demonstrated that continuous treatment with IL15 results in functional NK cell exhaustion (57). Therefore, in our approach, we performed a stable genetic modification of NK cells to continuously support them in the TME, regardless of the presence of cytokines. The strategy of genetic engineering of effector cells to promote their activity is an attractive approach already implemented in preclinical and clinical settings (58, 59). Moreover, NK-92 cells have already demonstrated potent effector function in preclinical models (60), and following irradiation, can also be safely administered in high doses to patients as an "off the shelf" cell therapy product (61).

Introduction of PRDX1 into adoptively transferred NK cells can have a broader antitumor effect beyond the protection of NK cells from oxidative stress, as was previously demonstrated for catalase-overexpressing CAR-modified T cells (62). Elimination of H_2O_2 by PRDX1-expressing NK cells can protect bystander immune cells and thereby modify the tumor's suppressive microenvironment. Although macrophages and neutrophils are largely resistant to high intracellular ROS, tumor-infiltrating T cells can be affected by oxidative stress. Specifically, several reports demonstrated apoptosis and downregulation of TCR/CD3z expression in T cells exposed to oxidative stress (63, 64). Therefore, the bystander effect of PRDX1-modified NK cells can indirectly provide a benefit for infiltrating T cells during the treatment of solid tumors.

In summary, our study demonstrates that increased H_2O_2 in the TME could have implications for immunotherapy treatment regimens, in particular those dependent on tumor-infiltrating NK cells or adoptively transferred NK cells. By characterization of antioxidant mechanisms in T, B, and NK cells, we highlighted PRDX1 as a lacking element of NK cells' antioxidative defense. Increasing the amount of PRDX1 in NK cells helped improve CAR NK cell activity against breast cancer cells under oxidative stress and is a basis for the development of new and more effective NK cell–based therapeutics against solid tumors.

Authors' Disclosures

M. Klopotowska reports personal fees from National Science Centre, Poland, and other support from Polpharma Scientific Foundation during the conduct of the study. M. Bajor reports grants from National Science Centre, Poland, during the conduct of the study. A. Graczyk-Jarzynka reports personal fees from National Science Centre, Poland, during the conduct of the study. A. Kraft reports personal fees from National Science Centre, Poland, and grants from Foundation for Polish Science during the conduct of the study. Z. Pilch reports personal fees from European Research Council during the conduct of the study. A. Zhylko reports personal fees from European Research Council during the conduct of the study. I. Baranowska reports personal fees from European Research Council during the conduct of the study. M. Lazniewski reports grants from Foundation for Polish Science, Warsaw University of Technology, and European and Developing Countries Clinical Trials Association during the conduct of the study. D. Plewczynski reports grants from Warsaw University of Technology, Polish National Science Centre, Foundation for Polish Science, and European and Developing Countries Clinical Trials Association during the conduct of the study. K. Soroczynska reports personal fees from European Research Council during the conduct of the study. M. Krawczyk reports personal fees from European Research Council during the conduct of the study. K.-J. Malmberg reports grants and personal fees from Fate Therapeutics, personal fees from Vycellix, and grants from Merck and Oncopeptides outside the submitted work. R. Zagozdzon reports grants and personal fees from National Science Centre, Poland; personal fees from Pure Biologics SA; and personal fees and other support from Helix Immuno-Oncology SA (currently 4Cell Therapies SA) and Medical Research Agency, Poland, outside the submitted work. M. Winiarska reports grants from National Science Centre, European Research Council, and The National Centre for Research and Development; other support from Polish Ministry of Science and Higher Education; and personal fees and other support from Polish Ministry of Science and Higher Education during the conduct of the study. No disclosures were reported by the other authors.

Authors' Contributions

M. Klopotowska: Conceptualization, resources, data curation, formal analysis, supervision, funding acquisition, validation, investigation, visualization, methodology, writing–original draft, project administration, writing–review and editing. **M. Bajor:** Conceptualization, data curation, formal analysis, validation, investigation, visualization, methodology, writing–review and editing. **A. Graczyk-Jarzynka:** Conceptualization, data curation, formal analysis, validation, investigation, visualization, methodology, writing–review and editing. **A. Kraft:** Data curation, formal analysis, validation, investigation, visualization, methodology, writing–review and editing. **Z. Pilch:** Conceptualization, investigation, visualization, methodology. **A. Zhylko:** Investigation, visualization, methodology, writing–review and editing. **M. Firczuk:** Conceptualization, data curation, writing–review and editing. **I. Baranowska:** Validation, investigation. **M. Lazniewski:** Conceptualization, investigation, writing–review and editing. **D. Plewczynski:** Conceptualization, investigation, visualization, methodology, writing–review and editing. **A. Goral:** Investigation, visualization, methodology, writing–review and editing. **K. Soroczynska:** Investigation, visualization, methodology. **J. Domagala:** Investigation, visualization, methodology, writing–review and editing. **K. Marhelava:** Investigation, visualization, methodology, writing–review and editing. **A. Slusarczyk:** Validation, investigation, visualization, methodology, writing–review and editing. **K. Retecki:** Validation, investigation, methodology, writing–review and editing. **K. Ramji:** Investigation, visualization, and methodology. **M. Krawczyk:** Investigation, visualization, methodology. **M.N. Temples:** Conceptualization, supervision, investigation, visualization, methodology, writing–review and editing. **B. Sharma:** Conceptualization,

resources, formal analysis, supervision, writing–original draft, writing–review and editing. **M. Lachota:** Conceptualization, resources, data curation, formal analysis, supervision, funding acquisition, investigation, visualization, methodology, writing–original draft, project administration, writing–review and editing. **H. Netskar:** Investigation, visualization, methodology. **K.-J. Malmberg:** Conceptualization, supervision, investigation, methodology, writing–review and editing. **R. Zagozdzon:** Conceptualization, formal analysis, investigation, visualization, methodology, writing–review and editing. **M. Winiarska:** Conceptualization, resources, data curation, formal analysis, supervision, funding acquisition, investigation, visualization, methodology, writing–original draft, project administration, writing–review and editing.

Acknowledgments

The authors thank Prof. Olaf Heidenreich from Princess Maxima Center, Utrecht, the Netherlands, for providing the pSLIEW-luc-GFP construct, Dr. Angelika Muchowicz for help with the orthotopic MCF-7 mammary fat pad murine model, and lab technicians Elżbieta Gutowska, Ewa Pięta, and Karolina Siudakowska for their help with PBMC isolations. The work was supported by grants from the National Science Centre (2015/19/B/NZ6/02862, M. Winiarska; 2019/33/B/NZ6/02503, M. Bajor), the European Research Council (grant number 805038/STIMUNO/ERC-2018-STG, M. Winiarska), and iONKO (Regionalna Inicjatywa Doskonalosci, grant number 013/RID/2018/19, 2019–2022, amount: 12 milion PLN) from the Polish Ministry of Education and Science. M. Winiarska is also supported by the Polish Ministry of Education and Science (419273/PnH/2018). M. Lazniewski, A. Kraft, and D. Plewczynski were supported by the Polish National Science Centre (2019/35/O/ST6/02484 and 2020/37/B/NZ2/03757) and Foundation for Polish Science cofinanced by the European Union under the European Regional Development Fund (TEAM to D. Plewczynski). M. Klopotowska received PhD scholarship sponsored by the Polpharma Scientific Foundation. M. Lazniewski was partially funded by IDUB against COVID-19 project granted by Warsaw University of Technology under the program Excellence Initiative: Research University (IDUB).

The costs of publication of this article were defrayed in part by the payment of page charges. This article must therefore be hereby marked *advertisement* in accordance with 18 U.S.C. Section 1734 solely to indicate this fact.

Received December 23, 2020; revised September 15, 2021; accepted November 30, 2021; published first December 1, 2021.

References

1. Daher M, Rezvani K. Outlook for new CAR-based therapies with a focus on CAR NK cells: what lies beyond CAR-engineered T cells in the race against cancer. Cancer Discov 2021;11:45–58.
2. Lupo KB, Matosevic S. Natural killer cells as allogeneic effectors in adoptive cancer immunotherapy. Cancers 2019;11:769.
3. Pahl JHW, Cerwenka A, Ni J. Memory-like NK cells: remembering a previous activation by cytokines and NK cell receptors. Front Immunol 2018;9:2796.
4. Domagala J, Lachota M, Klopotowska M, Graczyk-Jarzynka A, Domagala A, Zhylko A, et al. The tumor microenvironment—a metabolic obstacle to NK cells' activity. Cancers 2020;12:3542.
5. Giorgio M, Trinei M, Migliaccio E, Pelicci PG. Hydrogen peroxide: a metabolic by-product or a common mediator of ageing signals? Nat Rev Mol Cell Biol 2007;8:722–8.
6. Bienert GP, Schjoerring JK, Jahn TP. Membrane transport of hydrogen peroxide. Biochim Biophys Acta 2006;1758:994–1003.
7. Hopkins BL, Neumann CA. Redoxins as gatekeepers of the transcriptional oxidative stress response. Redox Biol 2019;21:101104.
8. Corzo CA, Cotter MJ, Cheng P, Cheng F, Kusmartsev S, Sotomayor E, et al. Mechanism regulating reactive oxygen species in tumor-induced myeloid-derived suppressor cells. J Immunol 2009;182:5693–701.
9. Sabharwal SS, Schumacker PT. Mitochondrial ROS in cancer: initiators, amplifiers or an Achilles' heel? Nat Rev Cancer 2014;14:709–21.
10. Sarmiento-Salinas FL, Delgado-Magallon A, Montes-Alvarado JB, Ramirez-Ramirez D, Flores-Alonso JC, Cortes-Hernandez P, et al. Breast cancer subtypes present a differential production of reactive oxygen species (ROS) and susceptibility to antioxidant treatment. Front Oncol 2019;9:480.
11. Winterbourn CC, Kettle AJ, Hampton MB. Reactive oxygen species and neutrophil function. Annu Rev Biochem 2016;85:765–92.
12. Canli O, Nicolas AM, Gupta J, Finkelmeier F, Goncharova O, Pesic M, et al. Myeloid cell-derived reactive oxygen species induce epithelial mutagenesis. Cancer Cell 2017;32:869–83.
13. Xiang H, Ramil CP, Hai J, Zhang C, Wang H, Watkins AA, et al. Cancer-associated fibroblasts promote immunosuppression by inducing ROS-generating monocytic MDSCs in lung squamous cell carcinoma. Cancer Immunol Res 2020;8:436–50.
14. Kono K, Salazar-Onfray F, Petersson M, Hansson J, Masucci G, Wasserman K, et al. Hydrogen peroxide secreted by tumor-derived macrophages down-modulates signal-transducing zeta molecules and inhibits tumor-specific T cell-and natural killer cell-mediated cytotoxicity. Eur J Immunol 1996;26:1308–13.
15. Izawa S, Kono K, Mimura K, Kawaguchi Y, Watanabe M, Maruyama T, et al. H(2)O(2) production within tumor microenvironment inversely correlated with infiltration of CD56(dim) NK cells in gastric and esophageal cancer: possible mechanisms of NK cell dysfunction. Cancer Immunol Immunother 2011;60:1801–10.
16. Hansson M, Asea A, Ersson U, Hermodsson S, Hellstrand K. Induction of apoptosis in NK cells by monocyte-derived reactive oxygen metabolites. J Immunol 1996;156:42–7.
17. Thoren FB, Romero AI, Hermodsson S, Hellstrand K. The CD16-/CD56bright subset of NK cells is resistant to oxidant-induced cell death. J Immunol 2007;179:781–5.
18. Harlin H, Hanson M, Johansson CC, Sakurai D, Poschke I, Norell H, et al. The CD16- CD56(bright) NK cell subset is resistant to reactive oxygen species produced by activated granulocytes and has higher antioxidative capacity than the CD16+ CD56(dim) subset. J Immunol 2007;179:4513–9.
19. Bauernhofer T, Kuss I, Henderson B, Baum AS, Whiteside TL. Preferential apoptosis of CD56dim natural killer cell subset in patients with cancer. Eur J Immunol 2003;33:119–24.
20. Winiarska M, Nowis D, Firczuk M, Zagozdzon A, Gabrysiak M, Sadowski R, et al. Selection of an optimal promoter for gene transfer in normal B cells. Mol Med Rep 2017;16:3041–8.
21. Demaison C, Parsley K, Brouns G, Scherr M, Battmer K, Kinnon C, et al. High-level transduction and gene expression in hematopoietic repopulating cells using a human immunodeficiency [correction of imunodeficiency] virus type 1-based lentiviral vector containing an internal spleen focus forming virus promoter. Hum Gene Ther 2002;13:803–13.
22. Martinez-Soria N, McKenzie L, Draper J, Ptasinska A, Issa H, Potluri S, et al. The oncogenic transcription factor RUNX1/ETO corrupts cell cycle regulation to drive leukemic transformation. Cancer Cell 2018;34:626–42.
23. Temples MN, Adjei IM, Nimocks PM, Djeu J, Sharma B. Engineered three-dimensional tumor models to study natural killer cell suppression. ACS Biomater Sci Eng 2020;6:4179–99.
24. Manders EMM, Verbeek FJ, Aten JA. Measurement of co-localization of objects in dual-colour confocal images. J Microsc 1993;169:375–82.
25. Wingett SW, Andrews S. FastQ Screen: a tool for multi-genome mapping and quality control. F1000Res 2018;7:1338.
26. Dobin A, Davis CA, Schlesinger F, Drenkow J, Zaleski C, Jha S, et al. STAR: ultrafast universal RNA-seq aligner. Bioinformatics 2012;29:15–21.
27. Li H, Handsaker B, Wysoker A, Fennell T, Ruan J, Homer N, et al. The sequence alignment/map format and SAMtools. Bioinformatics 2009;25:2078–9.
28. Liao Y, Smyth GK, Shi W. The R package Rsubread is easier, faster, cheaper and better for alignment and quantification of RNA sequencing reads. Nucleic Acids Res 2019;47:e47.
29. Leek JT, Johnson WE, Parker HS, Jaffe AE, Storey JD. The sva package for removing batch effects and other unwanted variation in high-throughput experiments. Bioinformatics 2012;28:882–3.
30. Wickham H. ggplot2. WIREs Computational Statistics 2011;3:180–5.
31. Anders S, Pyl PT, Huber W. HTSeq—a Python framework to work with high-throughput sequencing data. Bioinformatics 2015;31:166–9.
32. McCarthy DJ, Chen Y, Smyth GK. Differential expression analysis of multifactor RNA-Seq experiments with respect to biological variation. Nucleic Acids Res 2012;40:4288–97.
33. Robinson MD, McCarthy DJ, Smyth GK. edgeR: a Bioconductor package for differential expression analysis of digital gene expression data. Bioinformatics 2010;26:139–40.

34. Graczyk-Jarzynka A, Goral A, Muchowicz A, Zagozdzon R, Winiarska M, Bajor M, et al. Inhibition of thioredoxin-dependent H_2O_2 removal sensitizes malignant B-cells to pharmacological ascorbate. Redox Biol 2019;21:101062.
35. Antunes F, Cadenas E. Estimation of H_2O_2 gradients across biomembranes. FEBS Lett 2000;475:121–6.
36. Kalyanaraman B, Darley-Usmar V, Davies KJ, Dennery PA, Forman HJ, Grisham MB, et al. Measuring reactive oxygen and nitrogen species with fluorescent probes: challenges and limitations. Free Radic Biol Med 2012; 52:1–6.
37. Bidaux G, Borowiec AS, Gordienko D, Beck B, Shapovalov GG, Lemonnier L, et al. Epidermal TRPM8 channel isoform controls the balance between keratinocyte proliferation and differentiation in a cold-dependent manner. Proc Natl Acad Sci U S A 2015;112:E3345–54.
38. Yang Y, Neo SY, Chen Z, Cui W, Chen Y, Guo M, et al. Thioredoxin activity confers resistance against oxidative stress in tumor-infiltrating NK cells. J Clin Invest 2020;130:5508–22.
39. Huang BK, Sikes HD. Quantifying intracellular hydrogen peroxide perturbations in terms of concentration. Redox Biol 2014;2:955–62.
40. Fernandes AP, Holmgren A. Glutaredoxins: glutathione-dependent redox enzymes with functions far beyond a simple thioredoxin backup system. Antioxid Redox Signal 2004;6:63–74.
41. Neumann CA, Cao J, Manevich Y. Peroxiredoxin 1 and its role in cell signaling. Cell Cycle 2009;8:4072–8.
42. Liu E, Tong Y, Dotti G, Shaim H, Savoldo B, Mukherjee M, et al. Cord blood NK cells engineered to express IL-15 and a CD19-targeted CAR show long-term persistence and potent antitumor activity. Leukemia 2018;32:520–31.
43. Pfefferle A, Jacobs B, Netskar H, Ask EH, Lorenz S, Clancy T, et al. Intra-lineage plasticity and functional reprogramming maintain natural killer cell repertoire diversity. Cell Rep 2019;29:2284–94.
44. Mao Y, van Hoef V, Zhang X, Wennerberg E, Lorent J, Witt K, et al. IL-15 activates mTOR and primes stress-activated gene expression leading to prolonged antitumor capacity of NK cells. Blood 2016;128:1475–89.
45. Lunetti P, Di Giacomo M, Vergara D, De Domenico S, Maffia M, Zara V, et al. Metabolic reprogramming in breast cancer results in distinct mitochondrial bioenergetics between luminal and basal subtypes. FEBS J 2019;286: 688–709.
46. Davis ZB, Felices M, Verneris MR, Miller JS. Natural killer cell adoptive transfer therapy: exploiting the first line of defense against cancer. Cancer J 2015;21:486–91.
47. Aydin E, Johansson J, Nazir FH, Hellstrand K, Martner A. Role of NOX2-derived reactive oxygen species in NK cell-mediated control of murine melanoma metastasis. Cancer Immunol Res 2017;5:804–11.
48. Hansson M, Hermodsson S, Brune M, Mellqvist UH, Naredi P, Betten A, et al. Histamine protects T cells and natural killer cells against oxidative stress. J Interferon Cytokine Res 1999;19:1135–44.
49. Nakamura K, Matsunaga K. Susceptibility of natural killer (NK) cells to reactive oxygen species (ROS) and their restoration by the mimics of superoxide dismutase (SOD). Cancer Biother Radiopharm 1998;13:275–90.
50. Stiff A, Trikha P, Mundy-Bosse B, McMichael E, Mace TA, Benner B, et al. Nitric oxide production by myeloid-derived suppressor cells plays a role in impairing Fc receptor-mediated natural killer cell function. Clin Cancer Res 2018;24:1891–904.
51. Wang W, Erbe AK, Hank JA, Morris ZS, Sondel PM. NK cell-mediated antibody-dependent cellular cytotoxicity in cancer immunotherapy. Front Immunol 2015; 6:368.
52. Werlenius O, Aurelius J, Hallner A, Akhiani AA, Simpanen M, Martner A, et al. Reactive oxygen species induced by therapeutic CD20 antibodies inhibit natural killer cell-mediated antibody-dependent cellular cytotoxicity against primary CLL cells. Oncotarget 2016;7:32046–53.
53. Miller JS, Soignier Y, Panoskaltsis-Mortari A, McNearney SA, Yun GH, Fautsch SK, et al. Successful adoptive transfer and in vivo expansion of human haploidentical NK cells in patients with cancer. Blood 2005;105:3051–7.
54. Dunne J, Lynch S, O'Farrelly C, Todryk S, Hegarty JE, Feighery C, et al. Selective expansion and partial activation of human NK cells and NK receptor-positive T cells by IL-2 and IL-15. J Immunol 2001;167:3129–38.
55. Zhang M, Wen B, Anton OM, Yao Z, Dubois S, Ju W, et al. IL-15 enhanced antibody-dependent cellular cytotoxicity mediated by NK cells and macrophages. Proc Natl Acad Sci U S A 2018;115:E10915–E24.
56. Mimura K, Kua LF, Shimasaki N, Shiraishi K, Nakajima S, Siang LK, et al. Upregulation of thioredoxin-1 in activated human NK cells confers increased tolerance to oxidative stress. Cancer Immunol Immunother 2017;66:605–13.
57. Felices M, Lenvik AJ, McElmurry R, Chu S, Hinderlie P, Bendzick L, et al. Continuous treatment with IL-15 exhausts human NK cells via a metabolic defect. JCI Insight 2018;3:e96219.
58. Xie G, Dong H, Liang Y, Ham JD, Rizwan R, Chen J. CAR-NK cells: a promising cellular immunotherapy for cancer. EBioMedicine 2020;59:102975.
59. Jochems C, Hodge JW, Fantini M, Fujii R, Morillon YM, 2nd, Greiner JW, et al. An NK cell line (haNK) expressing high levels of granzyme and engineered to express the high affinity CD16 allele. Oncotarget 2016;7:86359–73.
60. Robbins Y, Greene S, Friedman J, Clavijo PE, Van Waes C, Fabian KP, et al. Tumor control via targeting PD-L1 with chimeric antigen receptor modified NK cells. Elife 2020;9:e54854.
61. Williams BA, Law AD, Routy B, denHollander N, Gupta V, Wang XH, et al. A phase I trial of NK-92 cells for refractory hematological malignancies relapsing after autologous hematopoietic cell transplantation shows safety and evidence of efficacy. Oncotarget 2017;8:89256–68.
62. Ligtenberg MA, Mougiakakos D, Mukhopadhyay M, Witt K, Lladser A, Chmielewski M, et al. Coexpressed catalase protects chimeric antigen receptor-redirected T cells as well as bystander cells from oxidative stress-induced loss of antitumor activity. J Immunol 2016;196:759–66.
63. Martner A, Aurelius J, Rydstrom A, Hellstrand K, Thoren FB. Redox remodeling by dendritic cells protects antigen-specific T cells against oxidative stress. J Immunol 2011;187:6243–8.
64. Nakagomi H, Petersson M, Magnusson I, Juhlin C, Matsuda M, Mellstedt H, et al. Decreased expression of the signal-transducing zeta chains in tumor-infiltrating T-cells and NK cells of patients with colorectal carcinoma. Cancer Res 1993;53: 5610–2.